Design of Substrate Integrated Waveguide H-plane Horn Antenna with Symmetric Beamwidths

by

Farzeen Iqbal
B.Eng., Nadirshaw Edulji Dinshaw University of Engineering and Technology, 2009

A Thesis Submitted in Partial Fulfillment of the
Requirements for the Degree of

MASTER OF APPLIED SCIENCE

in the Department of Electrical and Computer Engineering

Design of Substrate Integrated Waveguide H-plane Horn Antenna with Symmetric Beamwidths

by

Farzeen Iqbal
B.Eng., Nadirshaw Edulji Dinshaw University of Engineering and Technology, 2009

Supervisory Committee

Dr. Jens Bornemann, Supervisor
(Department of Electrical and Computer Engineering)

Dr. Poman So, Departmental Member
(Department of Electrical and Computer Engineering)

Supervisory Committee

Dr. Jens Bornemann, Supervisor
(Department of Electrical and Computer Engineering)

Dr. Poman So, Departmental Member
(Department of Electrical and Computer Engineering)

ABSTRACT

Millimeter-wave Substrate Integrated Waveguide (SIW) technology presents itself as the most viable solution for the development of RF systems. It is a cost-effective solution, suitable for mass production of such systems. Like planar circuits, SIW structures are compact, light weight and easy to fabricate. They also preserve some of the major advantages of metallic waveguides, namely, low loss, high quality factor and high power handling capabilities.

In RF systems, rectangular waveguide horns have found various applications due to their exceptional radiation properties. From their simple construction, ease of excitation, usefulness and high gain, they are readily used as feed component in various RF systems, they also aid as the standardization for calibration and gain measurements of other high gain antennas. We are aware that, in an H-plane horn antenna, the rectangular waveguide is flared in the direction of the H-field. A large aperture in the H-plane presents the narrower half power beamwidth whereas a small aperture in the E-plane gives a wider beamwidth. In this research, the design of a SIW H-plane horn antenna with approximately symmetric half power beamwidths in both the E- and H-planes is proposed, using the commercially available electromagnetic field solver CST Microwave Studio to design and simulate proposed antenna characteristics and performance. Also, radiation patterns are analyzed and in order to validate the simulation results, measurements are performed on a fabricated prototype antenna.

Contents

Supervisory Committee **ii**

Abstract **iii**

Table of Contents **iv**

List of Tables **vi**

List of Figures **vii**

Acknowledgements **ix**

Dedication **x**

1 Introduction **1**

1.1 Motivation 2

1.2 Contributions 3

1.3 Thesis Overview 3

2 Fundamental Concepts **5**

2.1 Important Antenna Parameters 5

2.1.1 Return Loss 5

2.1.2 Radiation Pattern 6

2.1.3 Beamwidth 6

2.1.4 Directivity 7

2.1.5 Gain 7

2.2 Horn Antenna 9

2.2.1 Rectangular waveguide 9

2.2.2 Horn Antenna Geometry 9

2.3 Substrate Integrated Waveguides 12

2.3.1 Design of Via Diameter and Via Separation 12
2.3.2 Equivalent Waveguide Width 14
2.3.3 Design of Substrate Integrated Waveguide Components 14
2.4 Radiating Slots 16

3 Performance Analysis of the SIW H-plane Horn Antenna 19
3.1 Horn Antenna Design Parameters 20
3.2 Analysis of Radiation Pattern in the E- and H-planes Using Simulated Results 21
3.2.1 Phase I: Simple SIW H-plane Horn Antenna 22
3.2.2 Phase II: H-plane Horn Antenna With Rectangular Slots . . . 23
3.2.2.1 Rectangular Slots: Dimensions and Position 25
3.2.2.2 Optimum Number of Slots: An Analysis 25
3.2.3 Phase III: Front-to-Back Ratio Enhancement in Slotted SIW H-plane Horn Antenna 26
3.2.4 S-parameter Analysis from Simulated Results 29
3.2.5 Phase IV: Addition of Printed Transition in Top Metallization 30
3.3 Inference from the Analysis 33

4 Measurements and Testing 35
4.1 Reflection Coefficient Measurement and Comparison 36
4.2 Radiation Pattern Measurement and Comparison 37

5 Conclusion 41

Bibliography 43

Appendix A: RT/duroid 5870 /5880 High Frequency Laminates 46

List of Tables

Table 3.1 H-plane dielectric horn dimensions (theoretical) 21
Table 3.2 SIW H-plane horn dimensions obtained from solver 21
Table 3.3 Performance comparison of the SIW H-plane horn antennas with and without slots 24
Table 3.4 Performance comparison of slotted SIW H-plane horn antennas with and without ground extension 28
Table 3.5 Performance comparison of simple H-plane horn antenna with slotted h-plane horn antenna (ground extension+transitions) . . 34

Table 4.1 Results comparison of the E- and H-plane simulated and measured radiation patterns 39

List of Figures

Figure 2.1 Co-ordinate system for antenna analysis [11] 6
Figure 2.2 E-field distribution in rectangular waveguide for $TE_{1,0}$ mode [13] 9
Figure 2.3 H-plane horn antenna geometry 10
Figure 2.4 Plot of function G_H versus A [11] 11
Figure 2.5 Plot of $a_1(\lambda)$ versus directivity [11] 11
Figure 2.6 Via diameter and hole separation 13
Figure 2.7 Structural parameters of the discontinuity between an all dielectric waveguide and the SIW structure [15] 14
Figure 2.8 Flow Chart for Design of SIW Component 15
Figure 2.9 Current distribution in a rectangular waveguide [17] 17
Figure 2.10Slots with no radiation 17
Figure 2.11Slots with radiation 18

Figure 3.1 H-plane horn antenna in CST Microwave Studio 22
Figure 3.2 E- and H-plane radiation patterns of SIW H-plane horn antenna 23
Figure 3.3 SIW H-plane horn antenna in CST Microwave Studio with slots 23
Figure 3.4 E- and H-plane radiation patterns of SIW H-plane horn antenna with slots 24
Figure 3.5 E-plane radiation pattern (left) , H-plane radiation pattern (right) for number of slots=3 26
Figure 3.6 E-plane radiation pattern (left), H-plane radiation pattern (right) for number of slots=4 26
Figure 3.7 Views of SIW slotted H-plane horn antenna with ground extension 27
Figure 3.8 Radiation patterns of Slotted SIW H-plane horn antenna with ground extension 28
Figure 3.9 Comparison of reflection coefficient at various stages of the design 29
Figure 3.10Comparison of reflection coefficient with and without transition 32

Figure 3.11Radiation patterns of the slotted SIW H-plane horn antenna with printed transition 33

Figure 4.1 SIW H-plane horn antenna prototype 36
Figure 4.2 S_{11} comparison, measured vs simulated 37
Figure 4.3 Anechoic Chamber 37
Figure 4.4 Radiation pattern comparison 38
Figure 4.5 E- and H-plane measured radiation patterns 39
Figure 4.6 Co-pol and cross-pol E- and H-plane radiation patterns 40

ACKNOWLEDGEMENTS

In my graduate research over the period of two years I have been supported by many people, I would like to take this opportunity to express my gratitude towards all of them.

My family, for showing their confidence in me and my abilities and supporting me whichever way possible from miles away.

Prof. Jens Bornemann, my supervisor , who had been extraordinarily supportive and tolerant, the door to his office was always open whenever I had a question about my research or writing. He always guided me in the right direction whenever he thought I needed it.

CADMIC Research Group Members, I appreciate them for all the talks that have helped me achieve my goals. I specially thank Ms. Mahbubeh Esmaeili to help me understand the software, CST Microwave Studio. I would also like to extend my gratitude to Ms. Sara Salem, she helped me understand how to perform measurements on the circuit and the do's and don't while doing it.

And once the storm is over, you won't remember how you made it through, how you managed to survive. You won't even be sure, whether the storm is really over. But one thing is certain. When you come out of the storm, you won't be the same person who walked in. That's what this storm's all about.
-Haruki Murakami

DEDICATION

I dedicate this thesis to my parents, I hope this accomplishment will complete the dream that you had for me, years ago when you chose to give me the best education you could.

Chapter 1

Introduction

For the evolution of RF systems, the implementation of millimeter-wave (mm-wave) integration technology is pivotal, which primarily depends on the availability of a cost-effective solution, suitable for mass production of such systems. In order to realize this objective, substrate integrated waveguide (SIW) technology presents itself as the most viable solution [1]. Substrate integrated waveguides are planar structures belonging to the family of substrate integrated circuits along with substrate integrated non-radiative dielectric waveguides (SINRDW) and substrate integrated image guide (SIIG) [2].

Like planar circuits, SIW structures are compact, light weight, easy to fabricate and cost effective. They also preserve some of the major advantages of metallic waveguides, namely, low loss, high quality factor and high power handling capabilities [1]. As far as the structure is concerned, in SIW components, the waveguide is fabricated by adding a top metal over a ground plane with sidewalls comprising of two rows of metallized vias embedded in a dielectric substrate. It can be viewed as a dielectric filled waveguide [2].

In RF systems, rectangular waveguide horns have found various applications due to their good radiation properties. From their simple construction, ease of excitation, usefulness and high gain, they are readily used as feed components to illuminate large radio astronomy dishes, satellite systems, and communication reflectors. Other than their utility as a feed for reflectors and lenses, they also aid as the standardization for calibration and gain measurements of other high gain antennas [3]. Three dimensional horn antennas are bulky in geometry but when constructed as the substrate integrated waveguide planar structure, they are both light in weight and have small volume.

A number of SIW planar horn designs have been proposed over the last decade.

For instance, a compact H-plane substrate integrated waveguide horn antenna design presented in [3] promises better antenna directivity using a dielectric arc lens and microstrip feed. The authors of [4] proposed a dielectric loaded millimeter wave H-plane horn antenna using low-temperature co-fired ceramic (LTCC) technology. Another design for radar application in the 21 GHz to 28 GHz frequency range is proposed in [5]; it utilizes a Polytetrafluoroethylene (PTFE) substrate and presents an increase of gain and narrower H-plane and E-plane beamwidths. And in a recent study [6], authors proposed uniform aperture distribution for a H-plane substrate integrated waveguide horn antenna. In [7], the authors present an improved E-plane radiation pattern from a coaxial-fed dual-layer SIW horn antenna design., this antenna has a 10-dB bandwidth of 5.37% and a gain of 10.33 dB at 21.5 GHz with E- and H-plane beamwidths of 73.8° and 27.6° respectively.

1.1 Motivation

In an H-plane horn antenna, the rectangular waveguide is flared in the direction of the H-field as compared to the E-plane horn antenna, where the flare is directed along the E-field. In the former, a large aperture in the H-plane presents the narrower beam whereas a small aperture in the E-plane gives a wider beam. This is opposite in the case of the E-plane horn antenna.

In this research, the design of a substrate integrated waveguide H-plane horn antenna with an approximately symmetric beamwidth in both the E- and H- planes is proposed, using the commercially available electromagnetic field solver CST Microwave Studio to design and simulate proposed antenna characteristics and performance. Radiation patterns are analyzed and in order to validate the simulation results, measurements are performed on a fabricated prototype antenna. The simulated results agree well with measured ones.

In the proposed design, two rectangular slots in the top metallization are inserted which radiate out the beam at an angle from the horizontal or the H-plane. This beam is approximately symmetric in both E- and H-planes, presenting higher gain and directivity along with narrow beamwidth as compared to simple substrate integrated H-plane horn antenna designs proposed previously. In previous research [8], a somewhat similar slotted H-plane horn antenna had been proposed with square slots, the main focus of that research was to maximize bandwidth and gain, and a two slots design presented maximum bandwidth of 800 MHz at 21.4 GHz. However,

measurements on a sample fabricated antenna were not provided.

1.2 Contributions

The contribution made by this research is twofold:

1. A new millimeter wave substrate integrated waveguide H-plane horn antenna is presented having approximately symmetric beamwidth, lower side lobe levels and less radiation towards the ground plane.

2. With 1 GHz bandwidth and 11.6 dB gain, compared to reported antennas in similar frequency ranges and with similar objectives, its performance indicates that it is more suitable for symmetric beamwidth applications than any of the other structures published so far.

3. Also, a research publication has been produced, entitled *Substrate Integrated Waveguide H-Plane Horn Antenna with Symmetric Beam*. The paper is submitted for presentation at the Asia Pacific Microwave Conference taking place in Kuala Lumpur, Malaysia in November, 2017.

1.3 Thesis Overview

This section outlines the structure of the thesis.

Chapter 2 describes fundamental concepts related to antennas in general, horn antenna design and substrate integrated waveguide (SIW) technology.

Chapter 3 discusses the outcomes of the proposed research obtained from CST Microwave Studio in detail. The first section describes the radiation pattern results in both E- and H-planes for a simple H-plane horn antenna design, followed by addition of slots in the top metallization and front-to-back ratio enhancement. The second section includes the s-parameter results at various stages and discusses how bandwidth enhancement is achieved along with front-to-back ratio.

Chapter 4 fully describes the measurements conducted on a prototype antenna. The results obtained are displayed with the support of necessary graphics as well as comparison is presented between the simulated and measured results.

Chapter 5 enumerates avenues of future work for further development of the concept and its applications.

Chapter 2

Fundamental Concepts

This chapter discusses important antenna parameters, horn antenna geometry, aperture, radiation fields and directivity of H-plane horn antennas as well as basics of substrate integrated waveguide (SIW) technology. We know that the antenna is a critical component of any RF communication system and by definition, it transmits and receives electromagnetic signals. In addition to this function, the antenna is designed in a way to accentuate the radiating signal in a particular direction and suppress it in all other directions. It can be said that the antenna functions as a directional device. Antennas can be of various sizes and shapes depending on design requirements and applications. It can be as simple as a conducting wire, an aperture, a patch, reflector or a lens and in the form of arrays [11]. Irrespective of the shape and size, we can say that the antenna is a transitional device between the transmission line and free space. The transmission line is a guided medium and can be a coaxial line or a waveguide.

2.1 Important Antenna Parameters

2.1.1 Return Loss

Return loss of an antenna in dB equals ten times the negative logarithm of the ratio of power reflected by the antenna to the power fed into the antenna through a transmission line. It is one of the most commonly used parameters in regards to antenna performance. It is related to the reflection coefficient Γ (also referred to as S_{11}) by

$$R_L = -20log_{10}\,|\Gamma| \tag{2.1}$$

2.1.2 Radiation Pattern

The radiation pattern is a graphical representation of the field or power radiated by the antenna in various directions. The radiation pattern is three-dimensional but it is most commonly represented in two dimensions, elevation and azimuth planes. In this thesis field patterns represent radiated electric or magnetic fields at a constant distance r from the antenna. Figure 2.1 shows the coordinate system for antenna analysis, where r , θ and ϕ are the variables in a spherical coordinate system.

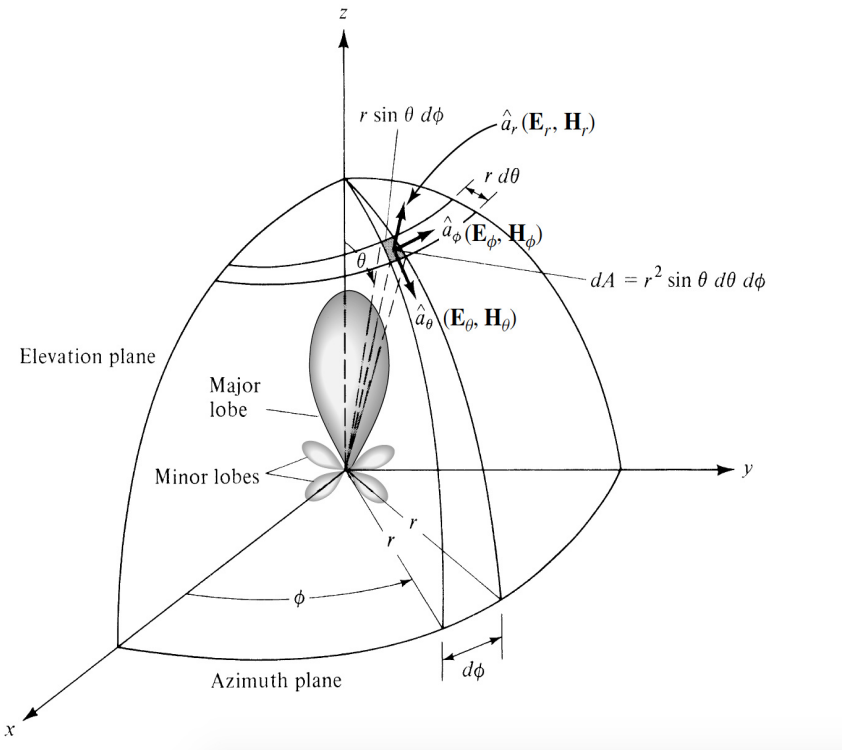

Figure 2.1: Co-ordinate system for antenna analysis [11]

2.1.3 Beamwidth

Beamwidth is defined with respect to the main lobe; it is the angular separation between two equal points on either direction of the lobe maximum. The narrower the beamwidth, the greater the gain of the antenna. But with a narrower beam, side lobe

levels increase. This makes beamwidth a very important parameter and is used as a trade-off for side lobe levels. Half power beamwidth (HPBW) is defined as angular separation between two half power points on the main beam. A different definition is the first null beamwidth (FNBW) which is the angular separation between first nulls of the radiation pattern [11].

2.1.4 Directivity

Mathematically, directivity is defined as [11]:

$$D = \frac{U}{U_0} = 4\pi \frac{U}{P_{rad}} \tag{2.2}$$

where,

U= radiation intensity in a given direction (W/ unit solid angle)
U_0= radiation intensity of isotropic source
P_{rad}= total power radiated (W)

If the direction is not given, then U is in the direction of maximum radiation and the directivity is said to be maximum directivity.

$$D_{max} = \frac{U_{max}}{U_0} = 4\pi \frac{U_{max}}{P_{rad}} \tag{2.3}$$

2.1.5 Gain

Antenna gain is one of the most useful parameters and can be defined in a number of ways [11],

$$Gain = \frac{U}{P_{in}} \tag{2.4}$$

where,

P_{in}= power accepted (input) by the antenna (W)

Equation 2.4 defines gain as the ratio of radiation intensity to the power accepted by the antenna. The input power to the antenna is the sum of the power radiated P_{rad} by the antenna and the power absorbed, P_{loss}, i.e.,

$$P_{in} = P_{rad} + P_{loss}, \tag{2.5}$$

Rewriting equation 2.3, we get:

$$Gain = \frac{U}{P_{rad} + P_{loss}} \tag{2.6}$$

Gain can also be defined as absolute gain (G_{abs}), which takes into account reflection (mismatch) losses in an antenna.

$$G_{0abs} = e_0 D_0 \tag{2.7}$$

where,

G_{0abs}= maximum absolute gain
D_0= maximum directivity
e_0= overall antenna efficiency

Overall antenna efficiency e_0 takes into account the losses at the input terminals and those within the structure of the antenna.

$$e_0 = e_r e_{cd} = e_{cd}(1 - \left|\Gamma^2\right|) \tag{2.8}$$

where,

e_r = reflection or mismatch efficiency
e_{cd}= radiation efficiency
Γ= reflection coefficient at antenna input terminals

IEEE definition of gain considers only radiation efficiency, i.e. e_{cd} [12], the conduction and dielectric efficiencies contribute to radiation efficiency, they are difficult to compute and can be determined experimentally but are difficult to separate (e_{cd}=e_c . e_d). In CST MWS, IEEE gain as well as realized gain is presented in far-field radiation patterns. As a rule of thumb for many practical antennas with narrow directional beams like horn antennas, gain is given by an approximation

$$G_0 = \frac{30,000}{\emptyset_1 \emptyset_2} \tag{2.9}$$

where, $\emptyset_1$ and $\emptyset_2$ are half power beamwidths in the two planes of an antenna.

2.2 Horn Antenna

Horn antennas are most widely used RF antennas. As mentioned earlier, they are used as a feed component for large radio astronomy dishes, satellite systems, and communication reflectors. A horn antenna is a simple hollow pipe of different cross sections, which is flared to a larger aperture. The direction and amount of flare has a great effect on the overall antenna performance. In an H-plane horn antenna, the waveguide is flared in the H-field direction, contrary to an E-plane horn antenna, where the rectangular waveguide is flared in the E-field direction.

In this thesis, an H-plane horn antenna design is proposed. Therefore, its detailed geometry is being discussed next.

2.2.1 Rectangular waveguide

Rectangular horn antennas are typically fed by a section of a waveguide, as shown in figure 2.2. It is simply a hollow, metallic cavity used to guide electromagnetic energy from one place to another, where a is the waveguide width, b is the waveguide height, the E-field distribution for the dominant mode or $TE_{1,0}$ in a rectangular waveguide is shown in figure 2.2.

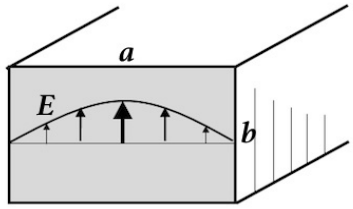

Figure 2.2: E-field distribution in rectangular waveguide for $TE_{1,0}$ mode [13]

A waveguide can support more than one propagation mode, the mode that propagates with the minimum degradation, i.e., the mode with the lowest cutoff frequency is called the Dominant Mode. Any frequency below cutoff fails to propagate through the rectangular waveguide, also the width a and the cutoff frequency f_c are inversely related with $f_c = c/(2a)$ for the dominant mode in the hollow metallic waveguide.

2.2.2 Horn Antenna Geometry

The detailed geometry of the H-plane horn antenna is shown in figure 2.3, a_1 is the aperture width and ψ is the angle at which the waveguide is flared in the H-plane.

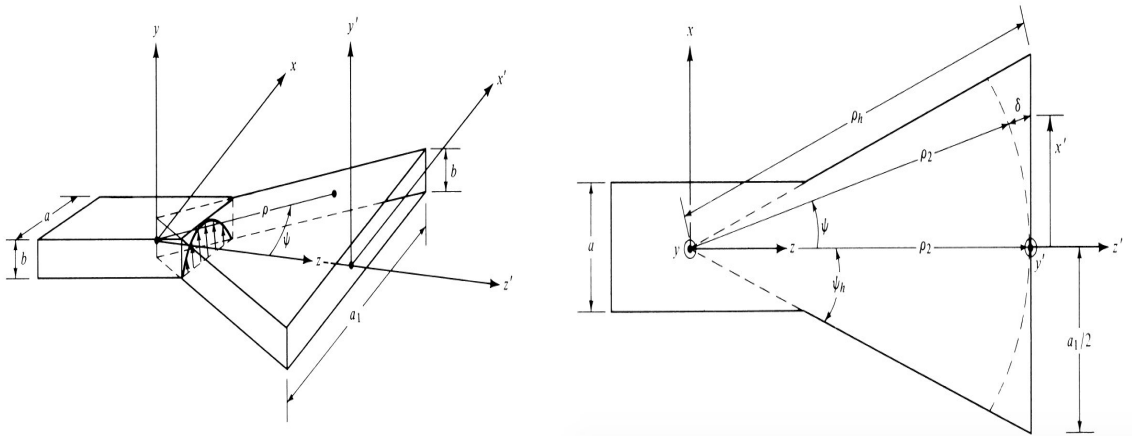

(a) Perspective View (b) Top View

Figure 2.3: H-plane horn antenna geometry

Figure 2.3(b) shows the top view of the H-plane horn antenna. Using the geometry described in figure 2.3, we can design an optimal H-plane horn antenna,

$$p_h = (a_1 - a)\sqrt{(\frac{\rho_h}{a_1})^2 - \frac{1}{4}} \tag{2.10a}$$

$$\rho_h = \rho_2^2 + (\frac{a_1}{2})^2 \tag{2.10b}$$

$$a_1 = \sqrt{3\lambda\rho_2} \tag{2.10c}$$

The directivity of an H-plane horn antenna can be calculated with the help of the following process [11]:

1. Calculate the term A:

$$A = \frac{a_1}{\lambda}\sqrt{\frac{50\lambda}{\rho_h}} \tag{2.11}$$

2. Now, using the value A determined from step 1, determine the value of function G_H from figure 2.4. If the value of A is smaller than 2, use the equation below to find G_H

$$G_H = \frac{32}{\pi}A \tag{2.12}$$

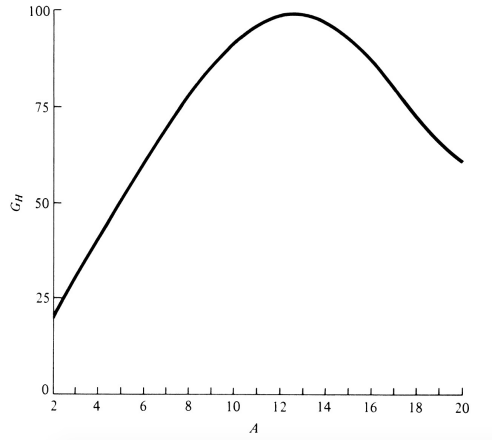

Figure 2.4: Plot of function G_H versus A [11]

3. Finally, calculate D_H from equation 2.12, using the value of G_H determined from step 2 and figure 2.5.

$$D_H = \frac{b}{\lambda} \frac{G_H}{\sqrt{\frac{50\lambda}{\rho_h}}} \tag{2.13}$$

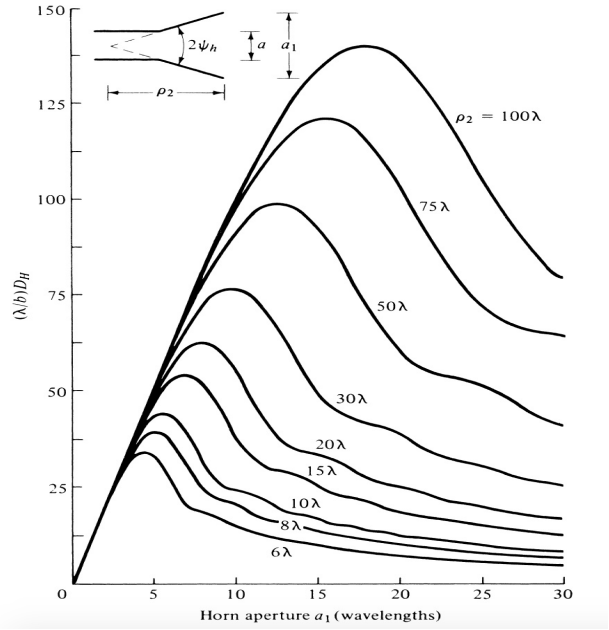

Figure 2.5: Plot of $a_1(\lambda)$ versus directivity [11]

In the previous section, equations 2.7 and 2.8 define the relationship between the gain and directivity.

In this thesis an H-plane substrate integrated waveguide (SIW) antenna is designed. Section 2.3 covers the fundamentals of SIW technology for the design of the proposed horn antenna.

2.3 Substrate Integrated Waveguides

As mentioned earlier, the substrate integrated waveguide is fabricated by adding a top metal over a ground plane with sidewalls comprising of two rows of metallized vias embedded in a dielectric substrate. It can be viewed as a dielectric filled waveguide [2]. Metallized via holes allow vertical currents to flow from the top to the bottom, and the space between holes, commonly referred to as *pitch*, stops longitudinal currents [14]. In substrate integrated waveguides only TE_{m0} modes are supported.

2.3.1 Design of Via Diameter and Via Separation

The detailed analysis has been performed in [14] in regards to the choice of via diameter and via separation. Practical design rules are obtained from the analysis, proposing suitable design parameters and regions for useful applications. Considering figure 2.6 (a) and (b), there is a region where a substrate integrated waveguide acts as its waveguide equivalent, with negligible leakage losses.

The region of interest is defined by following equations [14] :

$$p > d \tag{2.14a}$$

$$0.05 \leq \frac{p}{\lambda_c} \leq 0.25 \tag{2.14b}$$

$$0.5 \leq \frac{d}{p} \leq 0.83 \tag{2.14c}$$

According to equation 2.14(a), the pitch must be larger than the cylinder diameter so that the circuit is physically realizable. Equation 2.14(b) is required to avoid any band gap in the operating bandwidth and, for approximately zero leakage losses, equation 2.14(c) must be followed. It is also inferred that if the length of the pitch (i.e. separation between holes) is too small, the mechanical rigidity of the design is adversely affected. Therefore, the number of vias must be restricted to less than 20

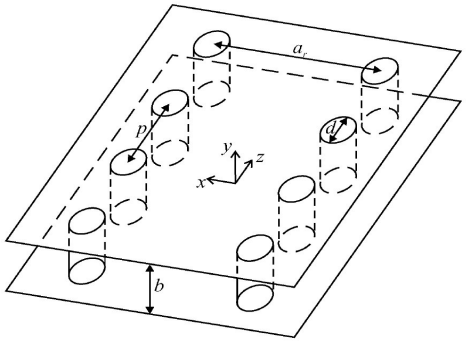

(a) Three dimensional view of SIW [14]

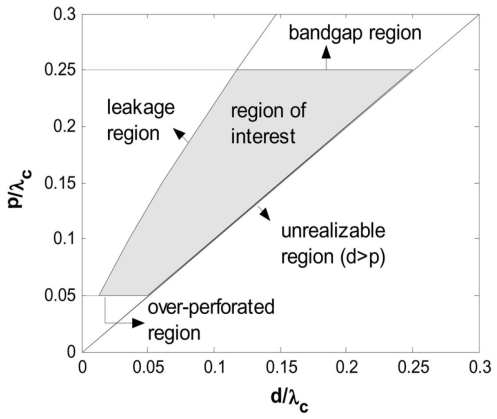

(b) Region of Interest for SIW design [14]

Figure 2.6: Via diameter and hole separation

per wavelength. In order to restrict dielectric and conductor losses, a $\frac{d}{p}$ ratio within $0.5< \frac{d}{p} < 0.83$ is recommended.

When the pitch, i.e. the spacing between vias increases, the electromagnetic field may no longer be restrained within the two rows of via cylinders. Some portion of this energy may now propagate outside these two via rows, thus resulting in the rise of leakage losses. These losses arise in the form of a coupling between the fundamental mode $TE_{1,0}$ and the parallel-plate mode.

Substrate integrated waveguide designs are prone to EM band-gaps or the stop-bands. While designing an SIW component it must be ensured that there are no band-gaps over the operating frequency range or bandwidth. The method presented in referred publication does not allow the determination of these band-gaps. But with the help of relation 2.14(b) it is possible to compute the maximum length of the pitch that is acceptable to avoid band-gaps in the operating range.

2.3.2 Equivalent Waveguide Width

The equivalent waveguide width determines the cutoff frequency in order to apply waveguide design procedures. Equation 2.15 is used for this purpose:

$$W_{equ} = \frac{c}{2f_c\sqrt{\epsilon_r}} \tag{2.15}$$

Various models have been developed to determine the equivalent width of SIW in the last two decades, the most recent one [15] calculates the equivalent width based on the design shown in figure 2.7.

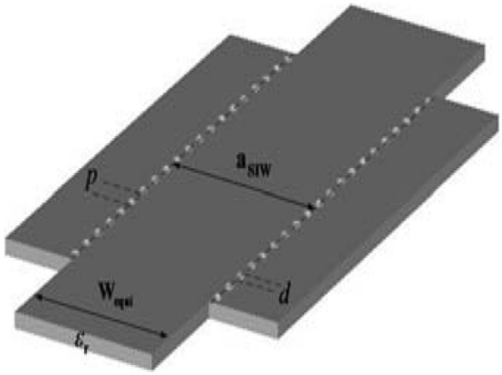

Figure 2.7: Structural parameters of the discontinuity between an all dielectric waveguide and the SIW structure [15]

The model developed in [15] gives the expression 2.16 for conversion between a_{SIW} and W_{equ} :

$$a_{SIW} = W_{equ} + p(0.766e^{0.4482\frac{d}{p}} - 1.176e^{1.214\frac{d}{p}}) \tag{2.16}$$

This model works for all practical ranges of $\frac{d}{p}$.

2.3.3 Design of Substrate Integrated Waveguide Components

In this thesis, for an H-plane horn antenna with slots, the design procedure in figure 2.8 [16] is followed:

1. For a given W_{equ}, i.e. the equivalent waveguide width for the SIW component, the cut-off frequency is calculated followed by determination of the operating frequency range 1.25 f_c - 1.9 f_c

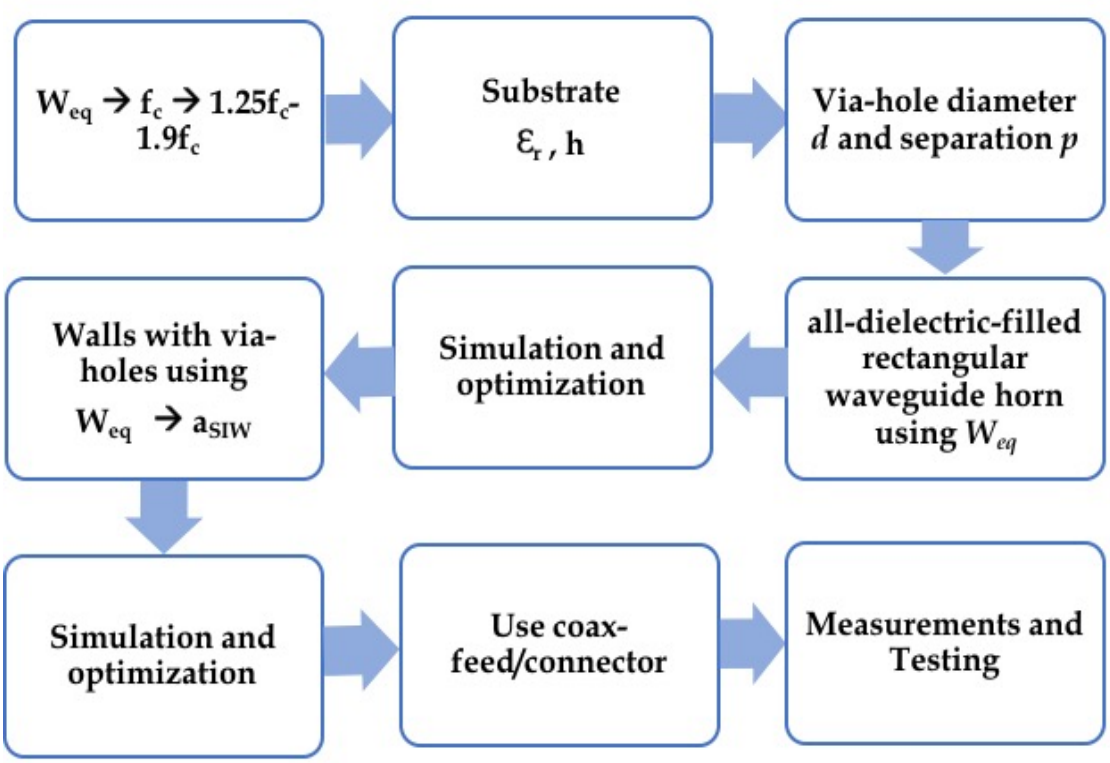

Figure 2.8: Flow Chart for Design of SIW Component

2. Substrate material and thickness h are determined based on the availability from manufacturers

3. Via-hole diameter and separation is determined within the range $0.5 < \frac{d}{p} < 0.8$, also, drill size availability at the manufacturer is checked

4. The required component is designed as an all-dielectric-filled rectangular waveguide H-plane horn using W_{equ}, considering via-hole thickness in certain parameters so that they can be replaced by holes later

5. Optimize the component for given specifications

6. Replace waveguide walls by via-holes using the equivalent waveguide to SIW width and a waveguide port

7. Optimize the SIW component again

8. Determine results with the selected coax-feed/connector

9. Perform required measurements once the component is fabricated

If we are working on a circuit based on a parameterized design, it might be fascinating to perceive how the results vary when some parameters are changed. The easiest procedure for acquiring these variation results is to perform a parameter sweep based analysis. Within the parameter sweep dialog box, we can modify the settings for a parameter sweep, including the parameters to be changed and the results to be observed during the sweep. Analysis through parameter sweep is much more flexible and takes much less time to analyze results, also results from each sweep are presented for observation.

In this thesis, for the horn antenna design, results produced by varying parameters like antenna taper angle/ aperture (a_1), position of coax feed and slot dimensions were analyzed using parameter sweep.

In comparison to parameter sweep, the optimizer in CST MWS, presents only *initial* and *best so far* results for the set goals, no results from intermediate steps are presented for analysis. However, the optimizer may be used to find optimal parameter settings for the design. Once the parametric values for anticipated results are obtained, we can use the optimizer to incorporate small variations in those dimensions. Optimization permits the designer to get the most out of the designed component or a circuit, as the small changes to a dimension of a component can have a significant effect on its tuning and efficiency.

2.4 Radiating Slots

In millimeter wave technology, structures such as dielectric waveguides have an open construction through which energy leakage is inevitable. This leakage occurs due to the discontinuities in the guiding structure, or when the waveguide is excited in an undesired mode. In terms of a leaky-wave antenna design, this energy leakage may be beneficial and can be exploited. This is achieved by purposefully creating discontinuities in the guiding structure such that the radiation is produced in a controlled manner. This antenna type is suitable for substrate integrated designs as they are well-suited with the waveguides from which they have originated. The most common example of these types of antenna is that of a slotted waveguide antenna, where the

current distribution in a waveguide is perturbed by inserting slots in the structure at a specific position.

The rectangular waveguides support both transverse electric (TE) or transverse magnetic (TM) modes of propagation, but their substrate integrated equivalents only allow $TE_{m,0}$ modes to propagate through the guide. Figure 2.9 shows the current distribution for a rectangular waveguide for the $TE_{1,0}$ mode.

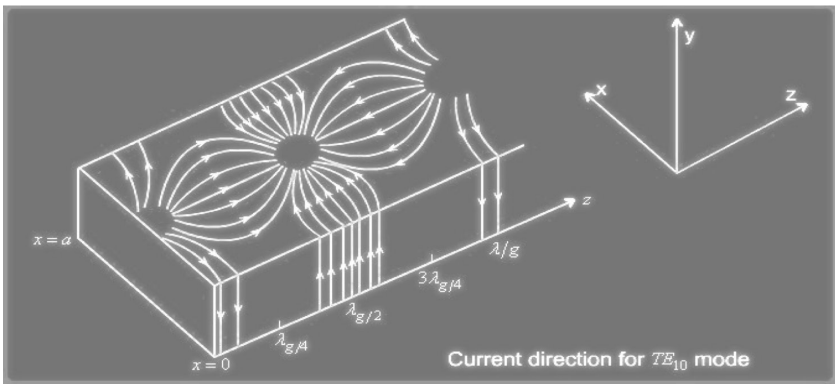

Figure 2.9: Current distribution in a rectangular waveguide [17]

The rectangular slots are cut into the walls of the guide to affect the flow of current, this depends on the location of the slots. In figure 2.10, the slots B and G have little or no influence on the current distribution. These two slots either not radiate or very little. A long slot at the center of the broad wall or a vertical slot in the side wall does not radiate.

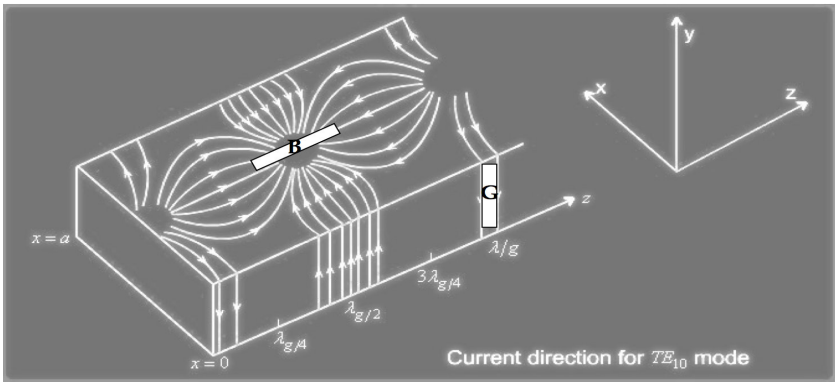

Figure 2.10: Slots with no radiation

For the slots to radiate the current flow must be perpendicular to the slots, i.e. magnetic field must be parallel. The slots A, C, D, E and F present a barrier to the current flow, this flow of current will act as an excitation system for these slots, and

they therefore radiate out. And, since the wave in the waveguide travels forward, these current lines that are drawn, drift in the direction of propagation.

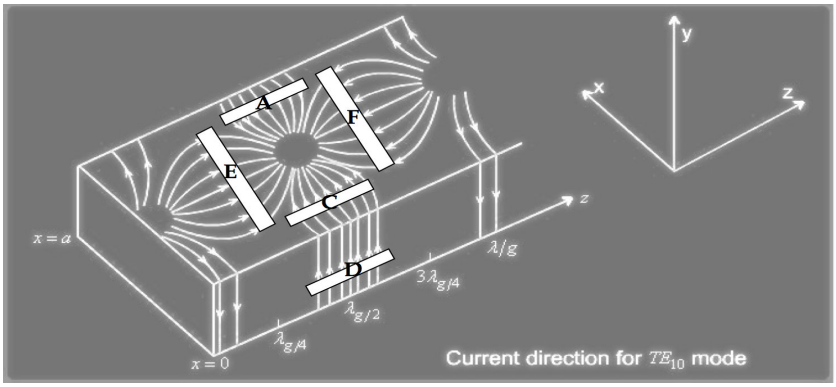

Figure 2.11: Slots with radiation

The null or the grey spots in the center of the broad wall occurs at $\lambda_g/4$ behind the shorted end of the guide. Slots must be placed such that they disturb the current distribution to cause radiation. In the proposed antenna design, two series slots are inserted in the top metallization of the antenna. These two slots are spaced at $\lambda_g/2$, where λ_g is the guide wavelength, which can be determined from $\lambda_g = \lambda_c/\sqrt{\epsilon_r}$, λ_c is the cutoff wavelength (for a cut-off frequency of 20 GHz), ϵ_r is the relative permittivity of the dielectric medium [18]. It is said that wider the antenna, greater the slot resonant bandwidth [19]. So the dimensions of the antenna, i.e. width, the spacing and length controls the amount of field radiated as well as the bandwidth of the antenna.

As mentioned, the distance between the last slot and the closed end of the guide is a quarter of a wavelength, transmission line theory states that a short circuit, a quarter wavelength down acts as open circuit, therefore slots are placed at these positions . Also, we know that slots are excited with electric current crossing it (or magnetic field along it). The intensity of current controls this excitation. When the current is normal to the slot (magnetic field is parallel), excitation is maximum and when the current is parallel to the slot (magnetic field is perpendicular) excitation is zero. Also, the smaller length of the slots weakens the excitation.

Chapter 3

Performance Analysis of the SIW H-plane Horn Antenna

The objective of this research is to design a substrate integrated waveguide H-plane horn antenna with approximately symmetric half power beamwidths in both the E- and H-planes, using the commercially available electromagnetic field solver CST Microwave Studio. In order to achieve this objective, two rectangular slots in the top metallization are inserted which radiate out the beam at an angle from the horizontal or the H-plane. This beam is approximately symmetric in both E- and H-planes, presenting higher gain and directivity along with narrower half power beamwidths as compared to simple substrate integrated waveguide H-plane horn antennas.

A similar approach was presented in [8] with the square slots in the top metallization. The main focus of that research was to maximize bandwidth and gain, this two square slots design presented a maximum bandwidth of 800 MHz at 21.4 GHz. However, the measurements on a sample fabricated antenna were not provided to support the simulation results. Authors in [9], presented dielectric loaded substrate integrated H-plane horn antennas, different shapes of dielectric loading were investigated, ellipse, rectangle, hyperbola and parabola. The rectangular dielectric slab gave the narrowest half power beamwidths in both E- and the H-planes and the highest gain with slightly higher side lobe level.

In [10], authors proposed a cost-effective way of reducing the side-lobe level and improving the front-to-back ratio of the substrate integrated waveguide H-plane horn antennas. Metal rectangular patches and dielectric loading were introduced to the aperture of the H-plane horn antenna, resulting in an increased gain, narrow E-plane

half power beamwidth, and reduced side-lobes and back lobe radiations. In [5], authors introduced the SIW H-plane horn antenna with dielectric loading resulting in improved gain and half power beamwidths on a PTFE substrate. In one of the recent study [6], authors proposed uniform aperture distribution for a H-plane substrate integrated waveguide horn antenna. In [7], the authors present an improved E-plane radiation pattern from a coaxial-fed dual-layer SIW horn antenna design., this antenna has a 10-dB bandwidth of 5.37% and a gain of 10.33 dB at 21.5 GHz with E- and H-plane beamwidths of 73.8° and 27.6°, respectively.

This chapter discusses the outcomes of the proposed research obtained from CST Microwave Studio in detail:

- The first section describes horn antenna design parameters obtained from equations discussed in chapter 2;
- The second section describes the radiation pattern results in both E- and H-planes for a simple SIW H-plane horn antenna design, followed by addition of slots in the top metallization and front-to-back ratio enhancement;
- The third section includes the s-parameter results on various stages and discusses how bandwidth enhancement is achieved along with front-to-back ratio.

3.1 Horn Antenna Design Parameters

Using the horn antenna design procedure, paramters are calculated as described in sections 2.2-2.4, important parameters are obtained from the equations. Table 3.1 provides these dimensions.

Parameter	Dimensions (mm)
Horn aperture	24.9940
Length of the horn flare	26
Equivalent waveguide width	4.9037
Cut-off Wavelength (λ_c)	9.8268
Guide Wavelength ($\lambda_g = \lambda_c/\sqrt{\epsilon_r}$)	6.4377
Diameter of vias	0.396875 = $\frac{1}{64''}$
Substrate height	1.575
Pitch	0.6
Offset between slots ($\lambda_g/2$)	3.218
Width of the slot ($\lambda_g/4$)	1.61
Length of the slot	8.047
Position of the first slot	17.709

Table 3.1: H-plane dielectric horn dimensions (theoretical)

3.2 Analysis of Radiation Pattern in the E- and H-planes Using Simulated Results

This section discusses the radiation patterns in both E- and H-planes in detail as obtained from simulations, from a simple SIW H-plane horn antenna to addition of rectangular slots in the top metallization and then to the extension of ground plane for front-to-back ratio enhancement.

Parameter	Dimensions (mm)
Horn aperture	25.5952
Length of the horn flare	26.3351
Equivalent waveguide width	4.9037
Diameter of vias	0.396875 = $\frac{1}{64''}$
Substrate height	1.575
Pitch	0.6
Offset (between slots)	3.9307
Width of the slot	1.96535
Length of the slot	8.3168
Position of the first slot	18.7176

Table 3.2: SIW H-plane horn dimensions obtained from solver

3.2.1 Phase I: Simple SIW H-plane Horn Antenna

Following the guidelines stated in section 2.3.3, for a given equivalent waveguide width for the SIW component, the cut-off frequency of 20 GHz is obtained from equation 2.14, followed by determination of the operating frequency range 1.25 f_c - 1.9 f_c, which comes out to be 25-38GHz. The substrate material and thickness h are determined based on the availability from manufacturers , RT/duroid 5870 with dielectric constant 2.33 and thickness 1.575 mm has been selected. Via-hole diameter and separation fall within the range $0.5 < \frac{d}{p} < 0.83$, also, the drill size availability at the manufacturer is checked. Table 3.2. presents the dimensions obtained from post optimization of various parameters to achieve the desired results from the electromagnetic field solver. Figure 3.1 (a)-(b) shows the top and back view of the SIW H-plane horn antenna designed in CST Microwave Studio.

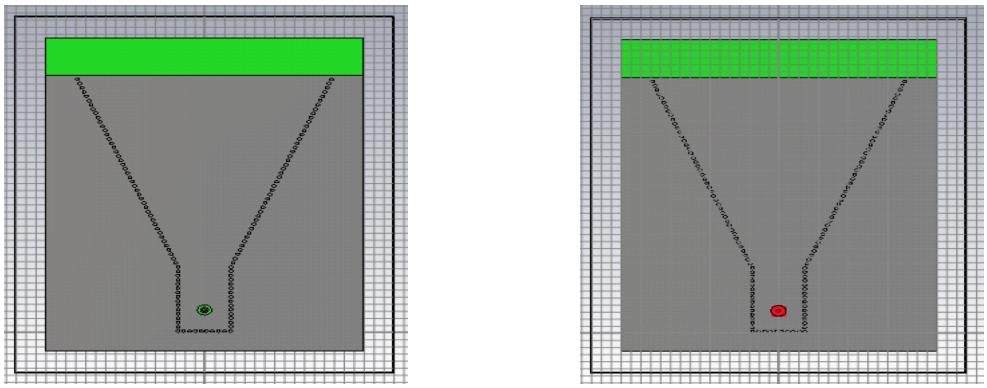

(a) Front (b) Back

Figure 3.1: H-plane horn antenna in CST Microwave Studio

Once the simulation is run, the E- and H-field radiation patterns are obtained as shown in figure 3.2 (a)-(b). At 26.3 GHz, a gain of 8.2 dB is obtained with H-plane and E-plane beamwidths of 30° and 126°, respectively. If we obtain the gain for the antenna using equation 2.9 and the beamwidths mentioned the gain comes out to be 8.99 dB, which is more than the gain presented by the field solver, however this is just a theoretical result from an approximation. From this phase of the design we can see that the beamwidth in the E-plane is much wider than that of the SIW H-plane for an H-plane horn antenna. Also the back lobe appears large, this may be due to the diffraction from antenna edges. Measures are taken to improve the front-to-back ratio in section 3.2.3.

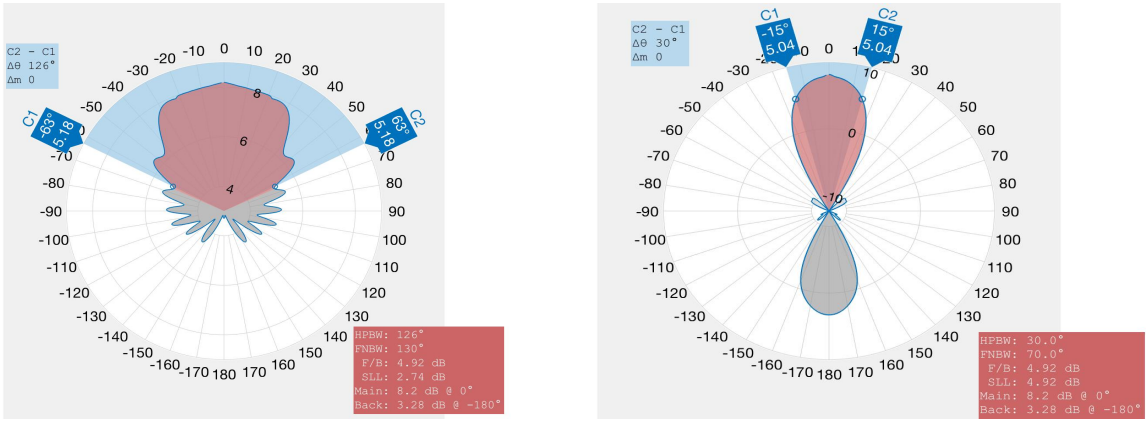

(a) E-field radiation pattern (b) H-field radiation pattern

Figure 3.2: E- and H-plane radiation patterns of SIW H-plane horn antenna

3.2.2 Phase II: H-plane Horn Antenna With Rectangular Slots

In order to achieve symmetric beamwidths in both the E- and H-planes, two rectangular slots are inserted in the top metallization according to the guidelines in section 2.4. These two slots radiate out field at an angle of 57° from the horizontal, resulting in the narrower half power beamwIdith of 28° in both the E- and H-planes. Figure 3.3(a)-(b) shows the top and back view of the antenna with two slots designed in CST.

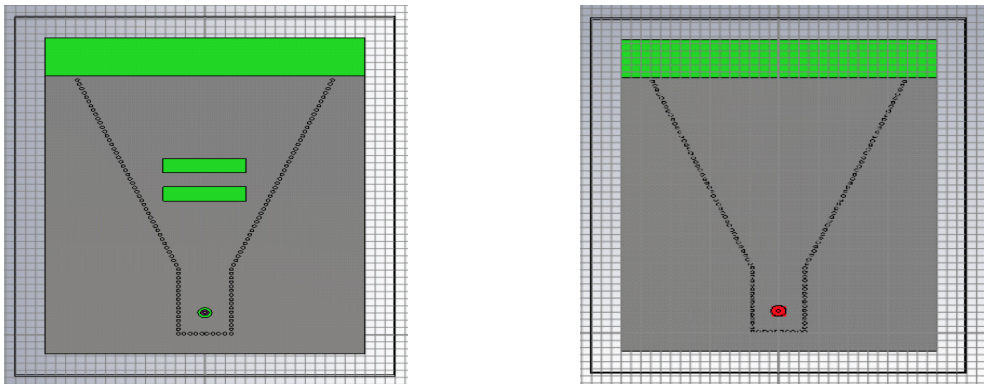

(a) Front (b) Back

Figure 3.3: SIW H-plane horn antenna in CST Microwave Studio with slots

The resulting radiation patterns in both the E- and H-planes are presented in figure 3.4(a)-(b). Table 3.3 compares the result between SIW H-plane horn antennas

with and without rectangular slots. We can see that there is a considerable increase in the gain when the slots are inserted in the top metallization of the H-plane horn antenna along with a resulting main beam inclined from the horizontal.

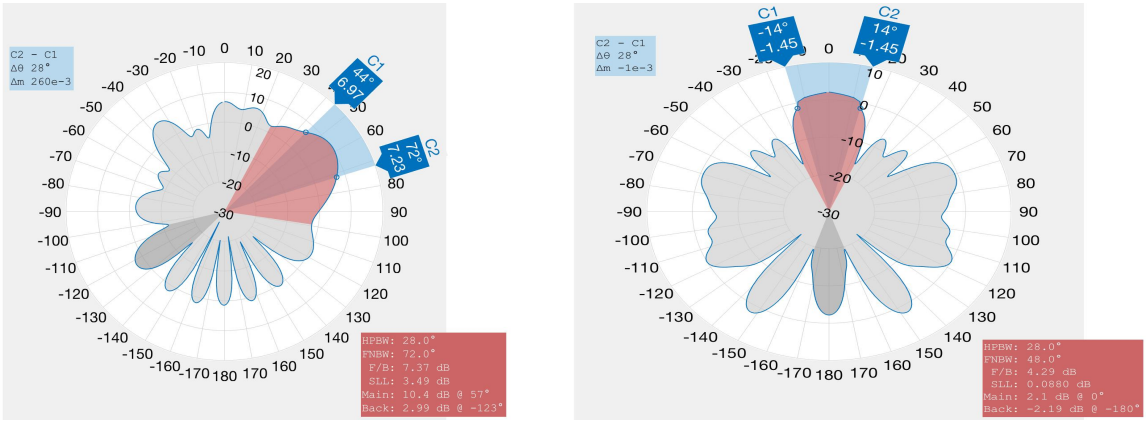

(a) E-field radiation pattern (b) H-field radiation pattern

Figure 3.4: E- and H-plane radiation patterns of SIW H-plane horn antenna with slots

Parameter	Without Slots	With Slots
Gain	8.2 dB	10.4 dB
Beam-width(H)	30°	28°
Beam-width(E)	126°	28°
Front to back ratio (H)	4.92 dB	4.29 dB
Front to back ratio (E)	4.92 dB	7.37 dB
Side lobe level (H)	4.92 dB	0.088 dB
Side lobe level (E)	2.74 dB	3.49 dB
Direction of the main beam	0°	57°

Table 3.3: Performance comparison of the SIW H-plane horn antennas with and without slots

Gain in the direction of the main beam has increased from 8.2 dB to 10.4 dB, the increased gain can be explained with the help of equations in section 2.1.4 and 2.1.5, where gain is directly related to radiation intensity in the direction of the main lobe. As the radiation intensity in the direction of the main lobe increases, so does the gain of the antenna. For a slotted H-plane horn antenna, the main lobe is directed at an angle from the horizontal. Also, the direction of the main lobe varies with the position of slots as well as the number of slots.

3.2.2.1 Rectangular Slots: Dimensions and Position

According to section 2.4, the rectangular slots are inserted with an offset of $\lambda_g/2$ between them, each slot has a width of $\lambda_g/4$. The distance between the slots or the offset is kept as $\lambda_g/2$, such that the slots will be fed in the same phase which is an equivalent electrical spacing of 180°. Therefore, each slot is exactly out of phase with its neighbours, so their radiations cancel each other, this results in the main beam which is inclined from the horizontal. For the position of the first slot (one closest to the source), the center of the slot is kept at a quarter wavelength away from the closed end of the waveguide. As we know that a short circuited quarter wavelength stub of transmission line works as an open-circuit, the closed end does not impact the impedance. However, in this case the start position is determined by $m * \lambda_g/4$, where an odd multiple of m is selected and optimized to obtain the desired radiation pattern. All dimensions are mentioned in Table 3.2.

3.2.2.2 Optimum Number of Slots: An Analysis

The number of slots in the top metallization were varied from two to four and radiation patterns in the E- and H-planes at 26.3 GHz are shown in figure 3.6 and It was observed that any number of slots greater than two resulted in higher side lobes in the E-plane and undesired main beam direction. The number of slots is used as a trade-off for the side lobe levels. In figure 3.5 (a)-(b), we see three rectangular slots in the top metallization. An increase in the side lobes is observed with the increase in number of slots, although the direction of the main beam remains the same along with narrow beamwidths in E- and H-planes of the antenna.

Now, if we look at figure 3.6(a)-(b) with four rectangular slots in the top metallization of the SIW H-plane horn antenna, the change in the direction of the main beam is observed, the main beam is now at a much greater angle from the horizontal (undesired direction). The direction of the main lobe does not vary from two to three slots but it changes drastically from 57° to −36°, when four slots are used.

Each of these transverse slots presents a reflection, which results in a radiation lobe located at −40°, a direction other than the main lobe direction when we compare figures 3.4-3.6 representing patterns obtained for possible number of slots from two to four. This lobe becomes significant as the number of slots is increased up-to four and the main lobe is no longer directed forward as presented in figure 3.5 (e) due to increased reflection from the slots.

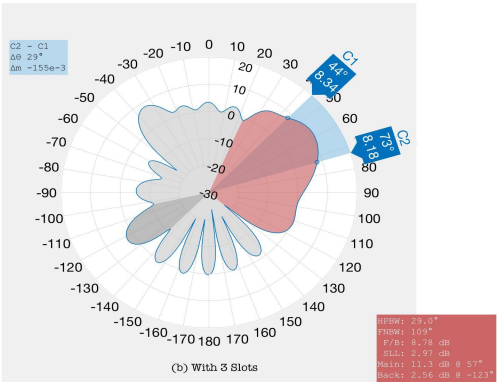

(a) With 3 Slots

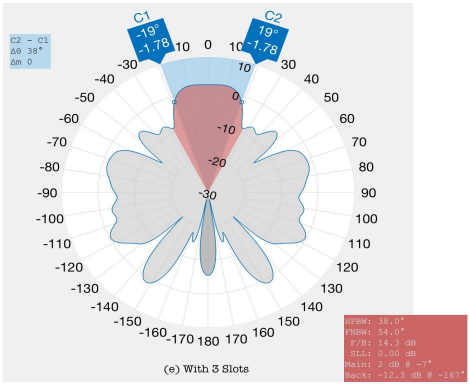

(b) With 3 Slots

Figure 3.5: E-plane radiation pattern (left) , H-plane radiation pattern (right) for number of slots=3

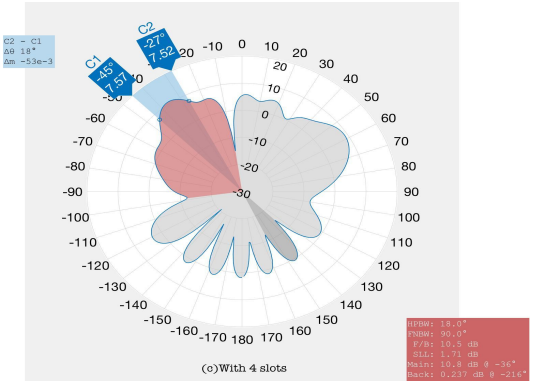

(a) With 4 Slots

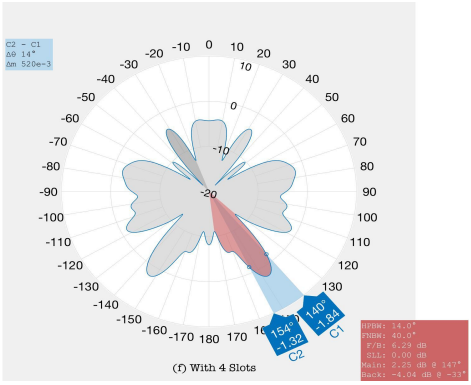

(b) With 4 Slots

Figure 3.6: E-plane radiation pattern (left), H-plane radiation pattern (right) for number of slots=4

After careful consideration of all parameters, including the side lobe level, back lobe, main beam, direction of the main beam and the half power beamwidths, it was deduced that the optimal number of slots in the top metallization is two.

3.2.3 Phase III: Front-to-Back Ratio Enhancement in Slotted SIW H-plane Horn Antenna

As indicated in figure 3.4 (a), the front-to-back ratio in the E-plane is 7.37 dB in the slotted H-plane horn antenna, as compared to figure 3.2 (a) of the simple horn antenna, where the front-to-back ratio is 4.92 dB. It is desired to have maximum radiation directed in the main lobe, therefore measures can be taken to enhance the

front-to-back ratio further.

In order to achieve this objective, the ground plane is extended up-to the length of the substrate, the length of the top metallization is kept as previously as shown in figure 3.7(a-c).

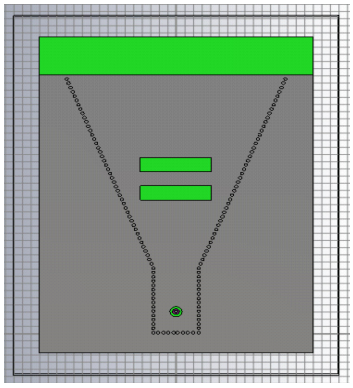

(a) Front

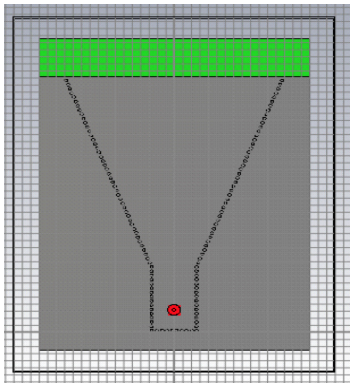

(b) Back without ground extension

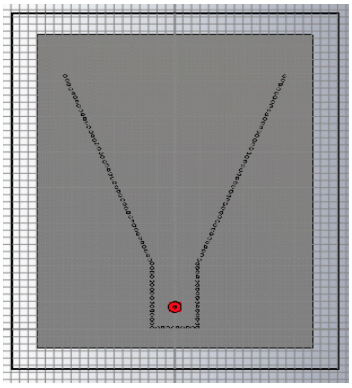

(c) Back with ground extension

Figure 3.7: Views of SIW slotted H-plane horn antenna with ground extension

This extension in the ground plane allows the field to travel farther in the substrate, reducing the back lobe level. This also reduces diffraction at the edge of the metallization, thereby enhancing the front-to-back ratio. In figure 3.8 (a)-(b), we see an increase in the gain of the main beam. This is due to the fact that, the ground extension resulted in decrease of the back lobe and now more energy/radiation is transmitted in the main lobe. The gain increased from 10.4 dB(without extension) to 11.9 dB (with extension). This observation can be explained on the basis of the gain equation 2.4, we see that gain is the ratio of radiation intensity in the given direction to the input power of the antenna. Due to ground extension, the radiation intensity is increased in the given/desired direction resulting in increased gain.

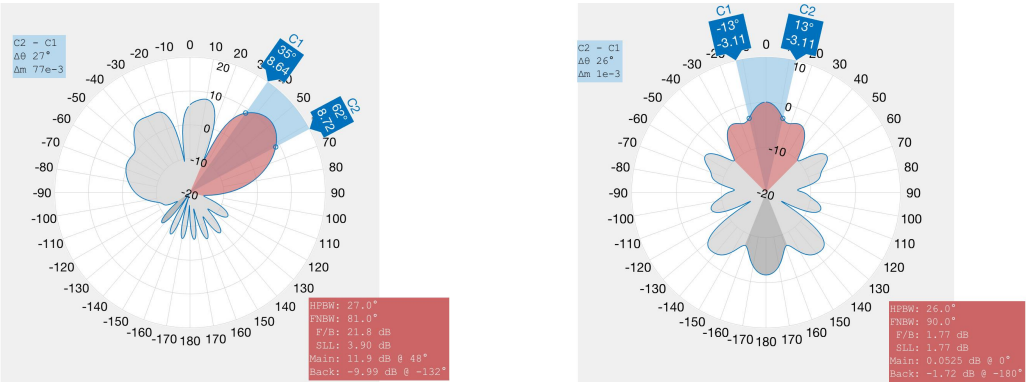

(a) E-field radiation pattern

(b) H-field radiation pattern

Figure 3.8: Radiation patterns of Slotted SIW H-plane horn antenna with ground extension

Comparing figure 3.4 (a) and 3.8 (a), we can say that in the E-plane, the main lobe level increased significantly, from 10.4 dB to 11.9 dB, the back lobe level reduced to -9.99 dB from 2.99 dB, and the front-to-back ratio increased comparably to 21.8 dB from 7.37 dB, without significantly affecting main lobe beamwidths in the two planes. But an increase in the side lobe level is observed. All these results are summarized in table 3.4. We can see that the main lobe is 9° closer to the horizontal plane, which justifies the purpose stated above that the field travels farther in the substrate as compared to the case without ground extension.

Parameter	**Without Extension**	**With Extension**
Gain	10.4 dB	11.9 dB
Beam-width(H)	28°	26°
Beam-width(E)	28°	27°
Front to back ratio (H)	4.29 dB	1.77 dB
Front to back ratio (E)	7.37 dB	21.8 dB
Side lobe level (H)	0.088 dB	1.77 dB
Side lobe level (E)	3.49 dB	3.9 dB
Direction of the main beam	57°	48°

Table 3.4: Performance comparison of slotted SIW H-plane horn antennas with and without ground extension

3.2.4 S-parameter Analysis from Simulated Results

The purpose of this thesis is twofold. First, to achieve symmetric beamwidths in both the E- and H-planes and second, to obtain ample bandwidth. The first objective has been covered in section 3.1 and 3.2 with detail. Now, in this section, s-parameter analysis is performed with an eye to obtain considerable bandwidth. Figure 3.9 compares S_{11} data obtained from simulations at various stages of the experiment over a wide range of frequency. Blue represents S_{11} for a simple SIW H-plane horn antenna discussed in section 3.2.1, red represents S_{11} for the horn antenna with two rectangular slots covered in section 3.2.2 and yellow represents S_{11} for the slotted SIW H-plane horn antenna with ground extension described in section 3.2.3.

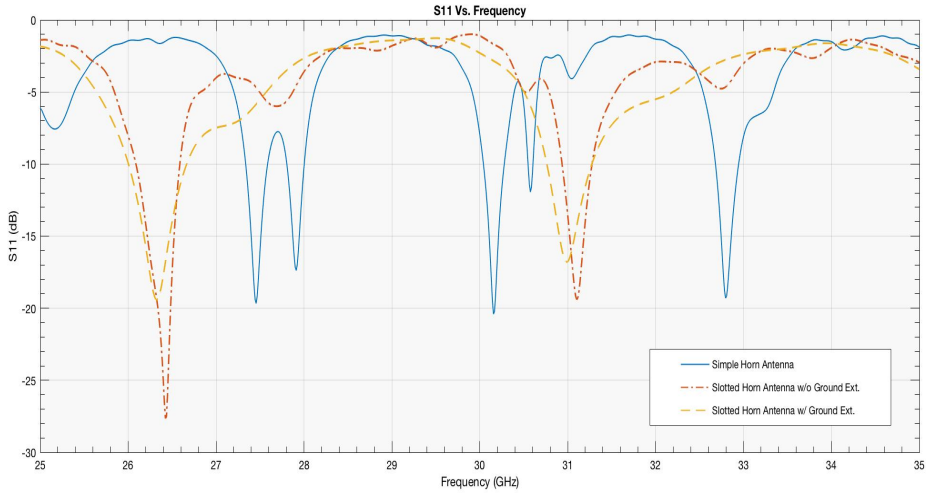

Figure 3.9: Comparison of reflection coefficient at various stages of the design

The S_{11} curve for a simple SIW H-plane horn antenna represents narrow bandwidth at frequencies of 27.5, 30.2 and 32.8 GHz. In order to obtain the first objective of this thesis, i.e. symmetric beamwidths in both the E- and H-planes, two rectangular slots are inserted in the top metallization as discussed in section 3.2.2, which results in the S_{11} curve shown in red. We can see that the S_{11} level considerably improves with a lower number of bands over the plotted frequency range, and we successfully observe symmetric beamwidths in the E- and H-planes. Now, in order to improve the front-to-back ratio, the ground plane is extended as described in section 3.2.3, the results indicate much greater improvement in front-to-back ratio but at the cost of reduced S_{11} level, represented by the yellow curve in figure 3.9. While in all three stages the bandwidth remained narrow, this is due to the fact that there is a

mismatch between the edge of the dielectric slab and the air, which decreases the operational bandwidth.

3.2.5 Phase IV: Addition of Printed Transition in Top Metallization

To achieve a good compromise between symmetric beamwidth and wider bandwidth, a printed transition consisting of two parallel plates/directors as implemented in [20] is considered. The authors propose a transition etched in the same dielectric substrate as that of the antenna, the working principle of these transitions is that of parallel-plate resonators separated from each other by distance s. The length of the transition can be calculated by equation 3.1 obtained from [21].

$$\frac{2\pi L}{\lambda_0} + \beta_{pp} L = (2n+1)\pi \tag{3.1}$$

and,

$$\beta_{pp} = \frac{2\pi\sqrt{\epsilon_{rpp}}}{\lambda_0} \tag{3.2}$$

β_{pp} is the propagation constant of parallel plate waveguides, and ϵ_{rpp} can be calculated from the quasi-static approximation presented in [22].The resonant frequency of one block is given by:

$$fr_1 = \frac{c}{2L_{eq}\sqrt{\epsilon_r}} \tag{3.3}$$

where L_{eq} is an equivalent length determined by the following equation:

$$L_{eq} = L(1 + \frac{0.7h}{L}) \tag{3.4}$$

The resonant frequency stated above shifts when two or more blocks are implemented. This is due to the fact that the coupling effect enhances and reduces the ability of a single block to store the charge. Since the blocks are separated by spacing s, two resonant frequencies fr_{2-} lower than fr_1 and fr_{2+} greater than fr_1 are generated. A coupling resonator k_2 is used to calculate $fr_2\pm$ using this equation:

$$fr_2\pm = \frac{fr_1}{\sqrt{1 \mp k_2}} \tag{3.5}$$

When two parallel plate transition blocks are concatenated, the capacitances produced by the gaps at the top and bottom planes contribute to the coupling effect. As

mentioned previously, this coupling effect enhances and thereby reduces the ability of a single block to store the charge, this results in a shift of resonant frequency, when the second pair of plates is inserted in top and ground plane. If Cs is the capacitance generated by the gap, with two blocks of parallel plates, there are two gaps in series. Therefore $Cc = Cs/2$, [20].

Where Cs is given as follows:

$$C_s(L_1, L_2) = \epsilon_0(\epsilon_r + 1)\frac{K(\sqrt{1 - p^2(L_1, L_2)})}{K(p(L_1, L_2))} \tag{3.6}$$

with,

$$p(L_1, L_2) = \sqrt{\frac{1 + \frac{L_1}{s} + \frac{L_2}{s}}{(1 + \frac{L_1}{s})(1 + \frac{L_2}{s})}} \tag{3.7}$$

where $K()$ is the complete elliptic integral of the first kind. The lengths of the transition plates at each side of the gap are represented by L_1 and L_2. For simplicity two equal length blocks are concatenated, which gives us L_1=L_2. The capacitance of the original structure is denoted by C_0, its value is now twice the capacitance of one parallel plates block, i.e. $2C_p$. C_p is the capacitance per unit length and is given by,

$$C_p \simeq \frac{\epsilon_0\epsilon_r h}{L}(1 + \frac{h}{\pi L} ln(\frac{\pi L}{h})) \tag{3.8}$$

Finally, the coupling factor k_2 for the case of two parallel transitions or blocks is calculated as follows:

$$k_2 = \frac{C_c}{C_0} = \frac{1}{2}\frac{C_s(L, L)}{2C_p} \tag{3.9}$$

In this thesis, the mathematical expressions stated above only provide a background for calculating the dimensions of the plates. Following dimensions were obtained, L_1=L_2=L= 2.4mm, L_{eq}= 3.552mm, fr_1= 27.66 GHz, fr_{2-}= 26.596 GHz, fr_{2+}= 29.115 GHz, k_2= 0.091, C_p= 42.52 pF, C_s= 15.469 pF. There is a discontinuity or a gap at the ground plane in the model presented above. No gap or discontinuity at the ground planes modifies the method utilized in the theory of coupled resonators for calculating fr_i. When the dimensions obtained from the described model in this section are implemented, they generated undesired or poor reflection coefficient performance. This may be attributed to the fact that the model stated above takes into account the gaps in the ground plane as well as the top plane, whereas, in the proposed antenna, gaps are only present in the top plane. Therefore, to obtain reasonable reflection coefficient performance, the calculated parameters were optimized

for bandwidth enhancement. After optimization, the values for the gap s_0 between the plates came out to be 0.189 mm and the length of the plates L_{eq} is 2.45 mm each.

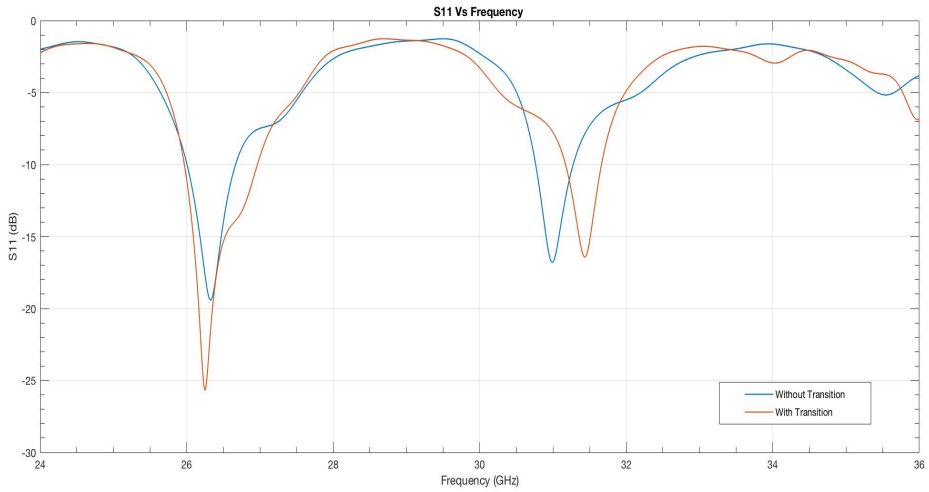

Figure 3.10: Comparison of reflection coefficient with and without transition

Also, the transmission zeros in the antenna's reflection co-efficient represents the number of parallel plate transitions. Since the length of both plates is the same, this should result in just one transmission zero at resonant frequency. However, it is to be noted in figure 3.10, there are two transmission zeros. These transmission zeros are due to the slots in the top plane of horn that radiate out field at an angle. The two transition plates did not vary the resonant frequency of the slots but only brought improvement in reflection coefficient level, front-to-back ratio and 10 dB return loss bandwidth.

The 10-dB return-loss bandwidth improved from 600 MHz without transitions to 1100 MHz with transition and the reflection coefficient improved to 25.6 dB from 18 dB at 26.3 GHz. There is a slight variation in the beamwidths of the E- and H-planes, they are now 33° and 22°, respectively, as shown in figure 3.11. There is a slight reduction in the gain too, from 11.9 dB to 11.6 dB. But overall a reasonable compromise has been achieved with narrow beamwidths in the two planes and improved bandwidth.

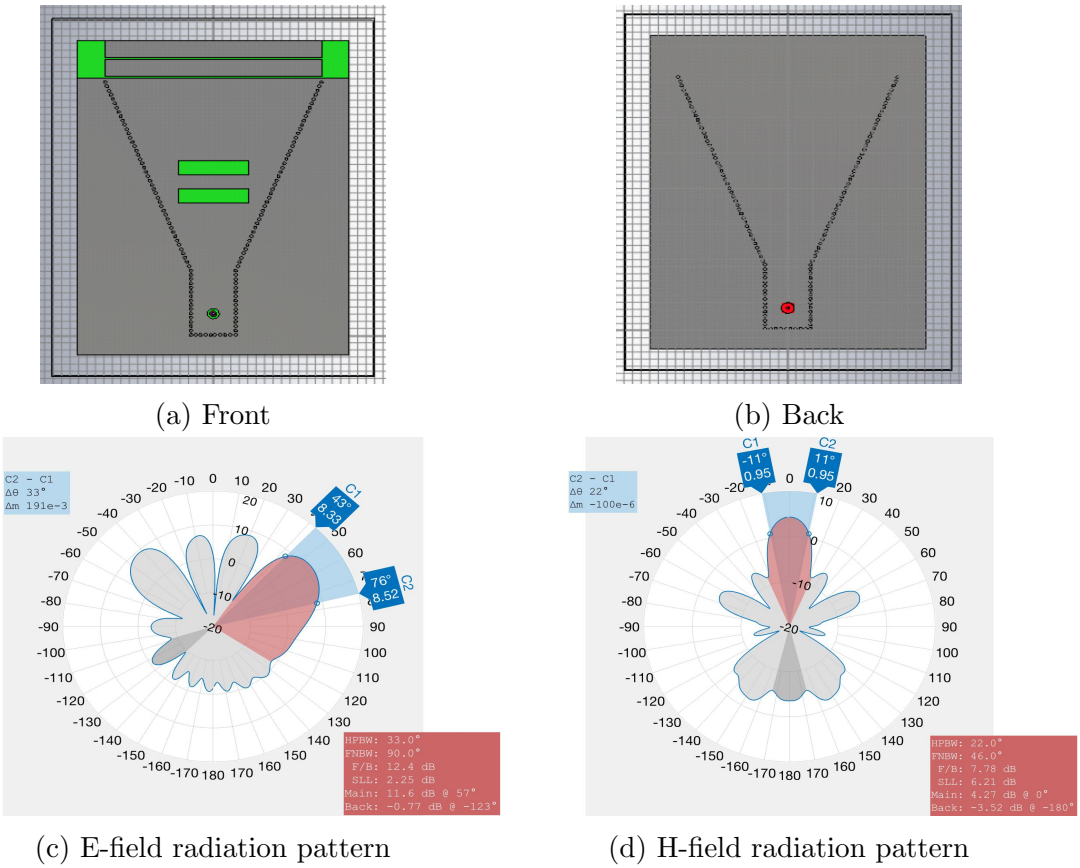

(a) Front (b) Back

(c) E-field radiation pattern (d) H-field radiation pattern

Figure 3.11: Radiation patterns of the slotted SIW H-plane horn antenna with printed transition

3.3 Inference from the Analysis

This section presents an inference deduced from the analysis phase of this thesis. Table 3.5 compares the radiation properties obtained from phase I of the simple H-plane horn antenna design to phase IV, where printed transitions were etched in a ground extended slotted horn antenna design.

When we compare the results obtained from the two phases presented in this table, we see that the gain of the ground extended slotted horn antenna with transitions presents better gain as compared to the simple horn antenna, gain of 11.6 dB is obtained as compared to the gain of 8.2 dB of the simple horn. The slots radiate out field at at angle of 57° from the horizontal, also, this main lobe has narrow half power beamwidths in the two planes (i.e. the E- and H-planes). The E-plane beamwidth of the simple horn antenna is 126°, which is much wider than the H-plane half power beamwidth of 30°. But for the ground extended slotted H-plane horn antenna (with

Parameter	**Phase I**	**Phase IV**
Gain	8.2 dB	11.6 dB
Beam-width(H)	30°	22°
Beam-width(E)	126°	33°
Front to back ratio (H)	4.92 dB	7.78 dB
Front to back ratio (E)	4.92 dB	12.4 dB
Side lobe level (H)	4.92 dB	6.21 dB
Side lobe level (E)	2.74 dB	2.25 dB
Direction of the main beam	0°	57°

Table 3.5: Performance comparison of simple H-plane horn antenna with slotted h-plane horn antenna (ground extension+transitions)

transitions), we can see that the two beamwidths are much narrower, they are now 22° and 33° in the H- and E-planes, respectively.

Also the front-to-back ratio has improved significantly with the help of the ground extension. However, there is a decrease in side lobe level observed from 2.74 dB to 2.25 dB in the E-plane specifically, which is indicative of the fact that as beamwidth gets narrower, side lobes increase. Also, an analysis with varying slot lengths was performed with the second slot larger than the first one but it failed to produce reasonable 10-dB return loss bandwidth performance, which can be attributed to increased reflection from the larger slot.

Chapter 4

Measurements and Testing

Once the design of a substrate integrated waveguide H-plane horn antenna is completed in CST Microwave Studio, its prototype is fabricated. Figure 4.1 shows the front and back views of this antenna prototype. The dimensions of this antenna prototype are 32 x 44 mm The antenna is fed using a coax connector, soldered into the board. In some circuits, soldering may be avoided and the circuit could be fed using a microstrip feed on a separate substrate layer or a coplanar waveguide from the backside. Two sets of measurements are performed, the input reflection coefficient and the radiation patterns of this antenna, and comparison is done with simulation results for verification.

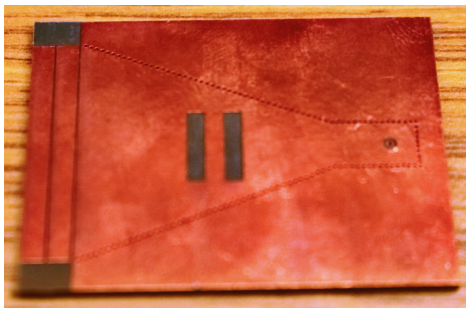

(a) Front

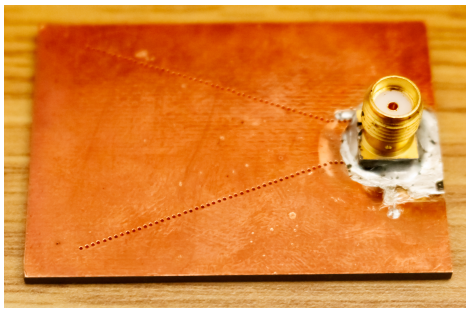

(b) Back

Figure 4.1: SIW H-plane horn antenna prototype

4.1 Reflection Coefficient Measurement and Comparison

The first measurement performed is that of the reflection coefficient, once the network analyzer is calibrated. Figure 4.2 compares the measured results with the simulated ones.

The blue solid line indicates the simulated results over the frequency range of 25-28 GHz, whereas the red dashed line represents the measured results. The simulation results present a 10 dB impedance bandwidth of 1GHz, i.e. 8.46 % and a reflection coefficient of 26 dB at 26.3 GHz. According to the measured results, a bandwidth of approximately 600 MHz, which is 4.62 %, with a reflection of coefficient of 25.02 dB at 26.3 GHz is obtained. The difference between the two curves is attributed to the coax connector and soldering. In the CST Microwave Studio, the coax connector is modelled as a perfect electric conductor, therefore it presents a narrower 10-dB return-loss bandwidth when measurements are performed on the prototype antenna.

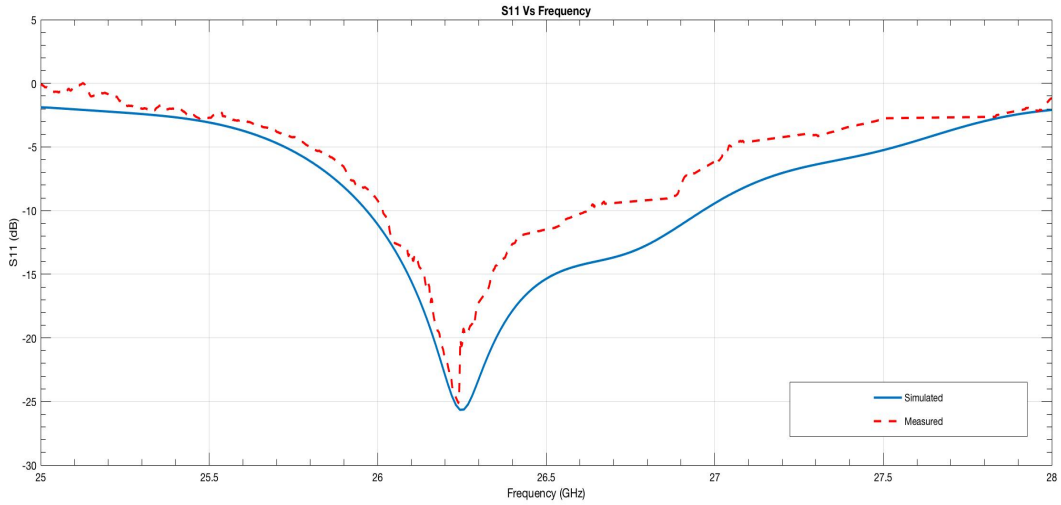

Figure 4.2: S_{11} comparison, measured vs simulated

4.2 Radiation Pattern Measurement and Comparison

The second set of measurements comprise of antenna radiation patterns in the far-field. This measurement is performed in an anechoic chamber as shown in Figure 4.3. This chamber is completely covered with pyramidal and walk-on absorbers which are made of radio absorbent material. The radiation patterns are measured by receiving the transmitted signal at different angles and various frequencies.

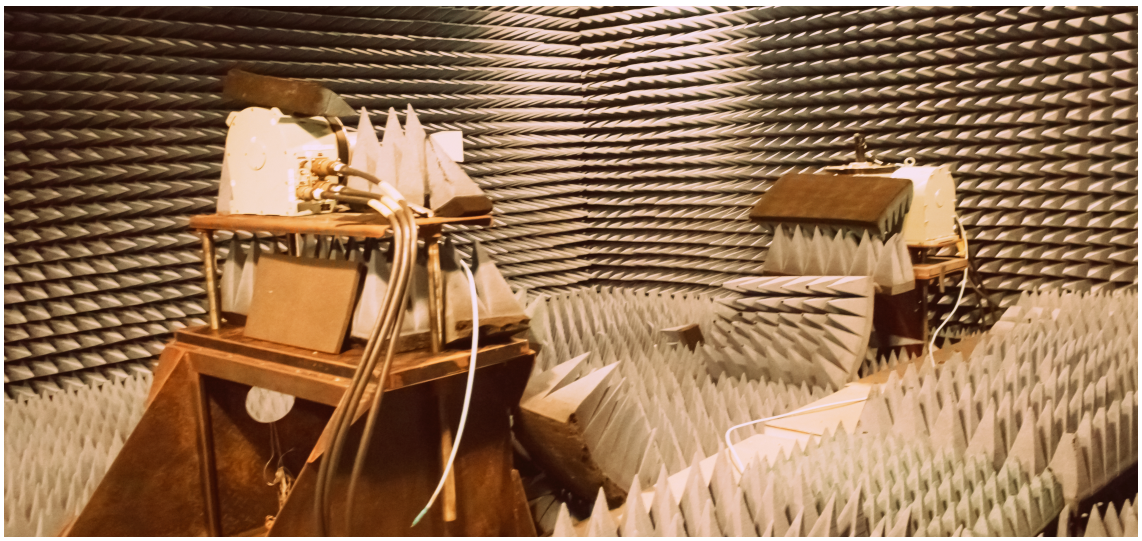

Figure 4.3: Anechoic Chamber

Figure 4.4 shows the comparison of the E- and H-plane radiation patterns at 26.3 GHz. Both measured and simulated results are in good agreement.

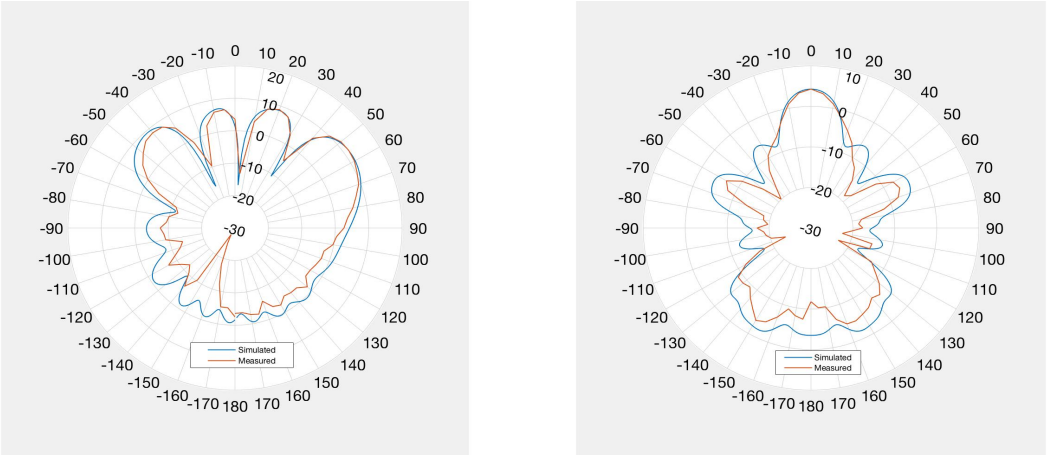

(a) E-plane (Co-polar) radiation pattern (b) H-plane (Co-polar) radiation pattern

Figure 4.4: Radiation pattern comparison

We can observe that, in the E-plane, the measured half power beamwidth (HPBW) at 26.3 GHz comes out to be 35° which agrees with the beamwidth of 33° obtained from simulation; similarly, the H-plane half power beamwidth (HPBW) is measured to be 20° as compared to 22° obtained from simulations. The main beam is directed at an angle of 55° from the horizontal as measured, which agrees with the direction of the main beam from simulated results. Figure 4.5 shows antenna measurements in both the E- and H-planes.

Table 4.1 drives a comparison between the simulated and measured results from figures 3.6 and 4.5.

Further analysis is performed by comparing the co- and cross-polar E- and H-plane radiation patterns. The measured E-plane co-pol and cross-pol patterns are shown in figure 4.6 (a).

The simulated half power beamwidth (HPBW) in the E-plane of the antenna is 35° which is well confirmed by measurement. A 37 dB isolation between the E-plane co-pol and cross-pol levels is measured in the main beam direction, slight asymmetry in the direction of patterns are attributed to the coax feed and attached cable which also influences cross-pol performance. Figure 4.6 (b) presents the measured and simulated H-plane co-pol and cross-pol patterns. The measured H-plane half power beamwidth (HPBW) of 20° is in good agreement with the simulated value of 22°. The measured H-plane cross-polar levels are higher than the simulated ones, which is attributed to

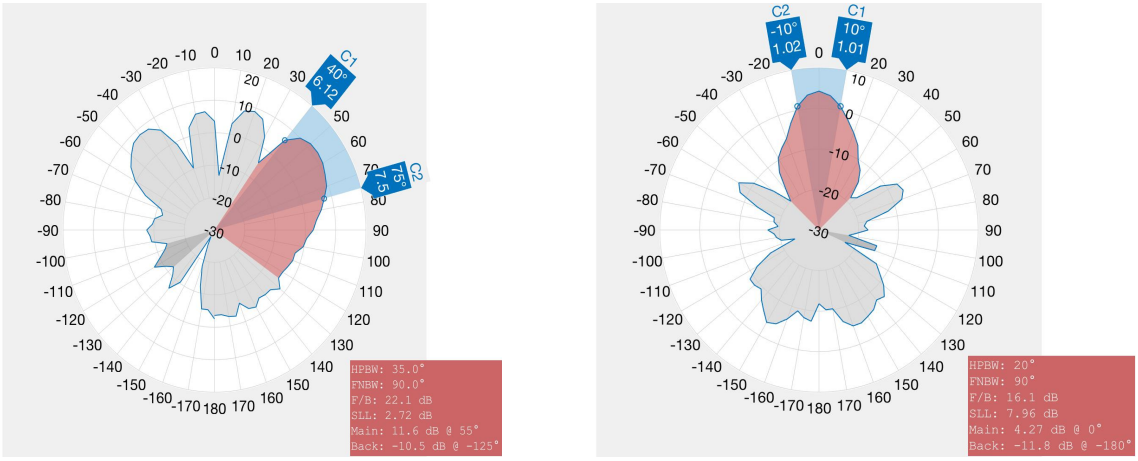

(a) E-plane (Co-polar) measured pattern (b) H-plane (Co-polar) measured pattern

Figure 4.5: E- and H-plane measured radiation patterns

Parameter	**Simulated**	**Measured**
Gain	11.6 dB	11.6 dB
Beam-width(H)	22°	20°
Beam-width(E)	33°	35°
Front to back ratio (H)	7.78 dB	16.1 dB
Front to back ratio (E)	12.4 dB	22.1 dB
Side lobe level (H)	6.21 dB	7.96 dB
Side lobe level (E)	2.25 dB	2.72 dB
Direction of the main beam	57°	55°

Table 4.1: Results comparison of the E- and H-plane simulated and measured radiation patterns

the metallic parts where the antenna is mounted that could not be entirely covered by absorber material.

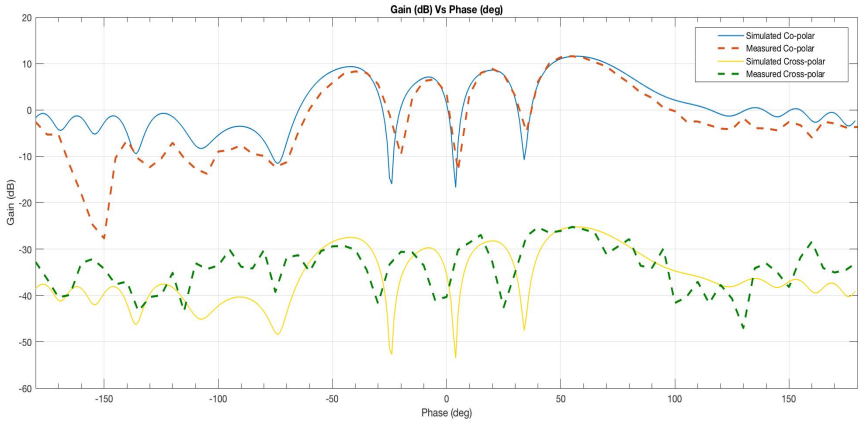

(a) E-plane

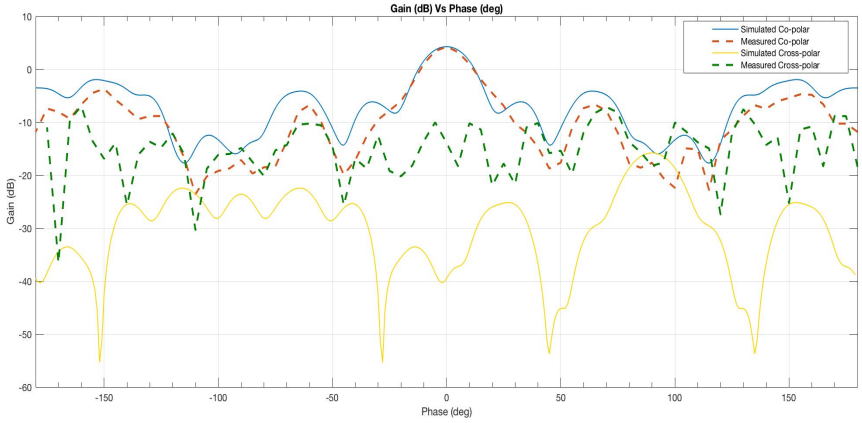

(b) H-plane

Figure 4.6: Co-pol and cross-pol E- and H-plane radiation patterns

Chapter 5

Conclusion

The applications of substrate integrated waveguides for microwave and millimeter wave integrated circuits has increased considerably over the last decade. They adopt the performance of a conventional hollow metallic waveguide and are fabricated using printed circuit boards with the top and bottom metallizations connected by two rows of vias forming the side walls. This technique creates a low profile, compact, and light weight alternative to conventional hollow metallic waveguide, and also allows connections with active components.

The development of millimeter wave technologies has led to a growing interest in SIW antennas. Several developed antenna topologies have been discussed in this thesis. SIW based antennas offer advantages similar to microstrip antennas as they can be fabricated with the same planar printed technology. Furthermore, SIW as a waveguide structure does not suffer from unintentional radiation and surface wave loss, which reduces the limitation of thin substrates. These merits make SIW a better candidate for antenna design.

Several slotted antennas have been proposed over the last decade. Radiation in SIW antennas is achieved by inserting slots in the top metallization of the structure. The very first slotted SIW antenna consisted of a four-by-four slotted SIW array operating at 10 GHz [23]. Recently, many designs of SIW slot antennas have been proposed with front-to-back ratio enhancement. The SIW slot antenna array based on comb-shaped chokes of quarter-wavelength parallel microstrip lines at the bottom surface of an array was stated to have lower back radiation by 10 dB [24]. An SIW slot antenna with folded corrugated stubs was proposed in [25] that resulted in suppressed back lobes. The concept of hollow SIW was implemented in a slotted waveguide antenna array presented in [26]. SIW slot antennas with broadband performance

were presented in [27] using the conventional log-periodic theory; results indicated a much wider impedance bandwidth as compared to conventional slotted waveguide antennas. Very few slotted horn antenna designs have been proposed to date, the one closest to this thesis is presented in [7] with square loop slots in the top metallization. This two square slots design presents a maximum bandwidth of 800 MHz at 21.4 GHz. However, measurements on a sample fabricated antenna were not provided to support the simulation results.

In this thesis, an SIW H-plane horn antenna with approximately symmetric beamwidths is proposed, designed and tested. The symmetric beamwidths is achieved by the insertion of two rectangular slots in the top metallization of the SIW H-plane horn antenna. Further measures have been taken to enhance front-to-back ratio and the 10-dB return-loss bandwidth. A reasonable compromise is achieved with narrow beamwidths in the two planes and improved bandwidth and front-to-back ratio. A bandwidth of approximately 600 MHz (4.62 %) as compared to 1 GHz bandwidth (8.46%) obtained from simulated results, with a reflection of coefficient of 25.02 dB at 26.3 GHz is obtained. HPBW's of 35° and 20° are measured in the E- and H-plane, respectively, as compared to 33° and 22° obtained form simulations, with a gain of 11.6 dB. Good agreement between simulated and measured results is observed, thus validating the proposed antenna design.

While the antenna itself encompasses all advantages of planar circuit fabrication, the coaxial feed adds a third dimension to the otherwise planar approach. Although simple microstrip feed structures have been investigated during the course of this work and have been found to fail to produce a satisfactory return loss band-width, several other feed structures, preferably on the opposite sides of the two slots, should be investigated. A coplanar waveguide feed structure with additional discontinuities to improve matching has recently been shown to provide a reasonable bandwidth for a circularly polarized SIW horn/dipole combination [28].

Bibliography

[1] M. Bozzi, L. Perredrini, K. Wu, P. Arcioni. *Current and Future Research Trends in Substrate Integrated Waveguide Technology*. RadioEngineering 18(2), pp. 201-209, Jun. 2009.

[2] K. Wu and D. Deslandes. *The Substrate Integrated Circuits-A New Concept for Hight-Frequency Electronics and Optoelectronics*. International Journal of RF and Microwave Computer-Aided Engineering, Nis, Yugoslavia, Yugoslavia, pp. III-X, Oct. 2003.

[3] W. Che, B. Fu, P. Yao, Y. L. Chow, E. K. N. Yung. *A Compact Substrate Integrated Waveguide H-plane Horn Antenna with Dielectric Arc Lens*, International Journal of RF and Microwave Computer-Aided Engineering, 17(5), pp. 473-479, Sept. 2007

[4] L. Yu and Q. Shi-Wei. *A Dielectric Loaded H-plane Horn for Millimeter Waves Based on LTCC Technology*, Cross Strait Quad-Regional Radio Science and Wireless Technology Conference, Chengdu, China, pp. 1-4, Jul. 2013.

[5] S. R. Ranade and D. U. Nair. *Design of Substrate Integrated Waveguide H-plane Horn Antenna on a PTFE Substrate for Automotive Radar Application*, Applied Electromagnetics Conference (AEMC), Kolkata, India, pp. 1-4, Dec. 2011.

[6] N. Bayat-Makao and A. A. Kishk. *Substrate Integrated Horn Antenna with Uniform Aperture Distribution*. IEEE Transactions on Antenna and Propagation 65(2), pp. 514-520, Feb. 2017.

[7] M. Esmaeili and J. Bornemann. *Coaxial-fed dual-layer SIW horn antenna with improved E-plane radiation pattern*. Proc. 47th Eur. Microw. Conf., Nuremberg, Germany, pp. 1-4, Oct. 2017.

[8] A. Patel, Alpesh Vala, R. Goswami, K. Mahant. *Square Loop Slots Loaded Substrate Integrated Waveguide Based Horn Antenna*. Microwave and Optical Technology Letters 58(7), pp. 1577-1582, Jul. 2016.

[9] Hao Wang, Da-Gang Fang, Bing Zhang, Wen-Quan Che. *Dielectric Loaded Substrate Integrated Waveguide (SIW) H-Plane Horn Antennas*. IEEE Transactions on Antenna and Propagation 58(3), pp. 640-647, Mar. 2010.

[10] Liang Gong, King Yuk Chan, Rodica Ramer. *Substrate Integrated Waveguide H-Plane Horn Antenna With Improved Front-to-Back Ratio and Reduced Side-lobe Level*, IEEE Antennas and Wireless Propagation Letters, 15 (2016) pp. 1835-1838.

[11] C. A. Balanis. *Antenna Theory- Analysis and Design*, John Wiley and Sons Inc., New York, Third Edition, 2005.

[12] J. Bornemann. *Lecture notes on Antenna and Propagation*, University of Victoria, Spring 2015.

[13] W. Frei *E-field distribution in rectangular waveguide for* $TE_{1,0}$ *mode*, https://www.comsol.com/blogs/ports-and-lumped-ports-for-wave-electromagnetics-problems/

[14] D. Deslandes and K. Wu. *Accurate Modelling , Wave Mechanisms, and Design Considerations of Substrate Integrated Waveguide*, IEEE Transactions on Microwave Theory and Techniques 54(6), pp. 2516-2526, Jun. 2006.

[15] Z. Kordiboroujeni and J. Bornemann. *Designing the Width of Substrate Integrated Waveguide Structures*, IEEE Transactions on Microwave and Wireless Components Letters 23(10), pp. 518-520, Oct. 2013.

[16] J. Bornemann. *Lecture notes on Theory and Design of Waveguide Components*, University of Victoria, Summer 2016.

[17] *Current distribution in a rectangular waveguide*, http://nptel.ac.in/courses/117101057/Slides-6/7.4.html

[18] J. Kachhia, A. Patel, A. Vala, R. Patel, K. Mahant *Logarithmic Slots Antennas Using Substrate Integrated Waveguide*, International Journal of Microwave Science and Technology, Vol.2015, Article ID 629797, pp. 1-11, Sept. 2015.

[19] R. L. Haupt *Antenna Arrays- A Computational Approach*, John Wiley and Sons Inc., New Jersey, 2010.

[20] M. Esquius Morote, B. Fuchs, J. Zurcher, J. Mosig. *A Printed Transition for Matching Improvement of SIW Horn Antennas*, IEEE Transactions on Antenna and Propagation, 61(4), pp. 1923-1930, Apr. 2013

[21] Y. Tang, Z. Wang, L. Xia, P. Chen. *A Novel High Gain K-band H-Plane SIW Horn Antenna Using Dielectric Loading*, Proc. of Asia-Pacific Microw. Conf., Sendai, Japan, pp. 372-374, Nov. 2014

[22] P. Benedek and P. Silvester. *Capacitance of Parallel Rectangular Plates Separated by a Dielectric Sheet*. IEEE Transactions on Microwave Theory and Techniques 20(8), pp. 504-510, Aug. 1972.

[23] L. Yan, W. Hong, G. Hua, J. Chen, K. Wu, T.J. Cui. *Simulation and Experiment on SIW Slot Array Antennas*, IEEE Microwave Wireless Component Letters 14 (2004), pp. 446-448.

[24] J. Wei, Z.N. Chen, X. Qing, J. Shi, J. Xu. *Compact Substrate Integrated Waveguide Slot Antenna Array with Low Back Lobe*, IEEE Antennas and Wireless Propagation Letters, 12 (2013) pp. 999-1002.

[25] D. Cho and H.Y. Lee. *Folded Corrugated SIW (FCSIW) Slot Antenna for Back-lobe Suppression*. IEEE Antennas Wireless Propagation Letters, 12 (2013), pp. 1276-1279.

[26] L. Jin, R. Lee, I. Robertson. *Analysis and Design of a Slotted Waveguide Antenna Array Using Hollow Substrate Integrated Waveguide*, European Microwave Conf., Paris, France, pp. 6-11, Sept. 2015.

[27] L. Jin, R. Lee, I. Robertson. *Design and Performance of log-periodic substrate integrated waveguide slot antennas*, IEEE MTT-S International Microwave Symposium Digest, Montreal, Canada, pp. 1-3, June 2012.

[28] Y. Luo and J. Bornemann. *Substrate integrated waveguide circularly polarized horn-dipole antenna with improved gain*, Microw. Opt. Technol. Lett., Vol. 58, pp. 2973-2977, Dec. 2016.

Appendix A

RT/duroid 5870 /5880 High Frequency Laminates

ROGERS CORPORATION

Data Sheet

RT/duroid® 5870 /5880
High Frequency Laminates

RT/duroid® 5870 and 5880 glass microfiber reinforced PTFE composites are designed for exacting stripline and microstrip circuit applications.

The randomly oriented microfibers result in exceptional dielectric constant uniformity.

The dielectric constant of RT/duroid 5870 and 5880 laminates is uniform from panel to panel and is constant over a wide frequency range.
Its low dissipation factor extends the usefulness of RT/duroid 5870 and 5880 laminates to Ku-band and above.

RT/duroid 5870 and 5880 laminates are easily cut, sheared and machined to shape. They are resistant to all solvents and reagents, hot or cold, normally used in etching printed circuits or in plating edges and holes.

Normally supplied as a laminate with electrodeposited copper of ½ to 2 ounces/ft.^{2} (8 to 70μm) or reverse treated EDC on both sides, RT/duroid 5870 and 5880 composites can also be clad with rolled copper foil for more critical electrical applications. Cladding with aluminum, copper or brass plate may also be specified.

When ordering RT/duroid 5870 and 5880 laminates, it is important to specify dielectric thickness, tolerance, rolled, electrodeposited or reverse treated copper foil, and weight of copper foil required.

Features:

- Lowest electrical loss for reinforced PTFE material
- Low moisture absorption
- Isotropic
- Uniform electrical properties over frequency
- Excellent chemical resistance

Some Typical Applications:

- Commercial Airline Broadband Antennas
- Microstrip and Stripline Circuits
- Millimeter Wave Applications
- Military Radar Systems
- Missile Guidance Systems
- Point to Point Digital Radio Antennas

Advanced Connectivity Solutions
100 S. Roosevelt Avenue, Chandler, AZ 85226
Tel: 480-961-1382 Fax: 480-961-4533 www.rogerscorp.com

PROPERTY	TYPICAL VALUES RT/duroid 5870		RT/duroid 5880		DIRECTION	UNITS[3]	CONDITION	TEST METHOD
[1]Dielectric Constant, ε_r Process	2.33 2.33 ± 0.02 spec.		2.20 2.20 ± 0.02 spec.		Z Z	N/A	C24/23/50 C24/23/50	1 MHz IPC-TM-650 2.5.5.3 10 GHz IPC-TM 2.5.5.5
[4]Dielectric Constant, ε_r Design	2.33		2.20		Z	N/A	8 GHz - 40 GHz	Differential Phase Length Method
Dissipation Factor, tan δ	0.0005 0.0012		0.0004 0.0009		Z Z	N/A	C24/23/50 C24/23/50	1 MHz IPC-TM-650, 2.5.5.3 10 GHz IPC-TM-2.5.5.5
Thermal Coefficient of ε_r	-115		-125		Z	ppm/°C	-50 - 150°C	IPC-TM-650, 2.5.5.5
Volume Resistivity	2 X 10^7		2 X 10^7		Z	Mohm cm	C96/35/90	ASTM D257
Surface Resistivity	2 X 10^7		3 X 10^7		Z	Mohm	C/96/35/90	ASTM D257
Specific Heat	0.96 (0.23)		0.96 (0.23)		N/A	J/g/K (cal/g/C)	N/A	Calculated
Tensile Modulus	Test at 23 °C	Test at 100 °C	Test at 23 °C	Test at 100 °C	N/A	MPa (kpsi)	A	ASTM D638
	1300 (189)	490 (71)	1070 (156)	450 (65)	X			
	1280 (185)	430 (63)	860 (125)	380 (55)	Y			
ultimate stress	50 (7.3)	34 (4.8)	29 (4.2)	20 (2.9)	X			
	42 (6.1)	34 (4.8)	27 (3.9)	18 (2.6)	Y			
ultimate strain	9.8	8.7	6.0	7.2	X	%		
	9.8	8.6	4.9	5.8	Y			
Compressive Modulus	1210 (176)	680 (99)	710 (103)	500 (73)	X	MPa (kpsi)	A	ASTM D695
	1360 (198)	860 (125)	710 (103)	500 (73)	Y			
	803 (120)	520 (76)	940 (136)	670 (97)	Z			
ultimate stress	30 (4.4)	23 (3.4)	27 (3.9)	22 (3.2)	X			
	37 (5.3)	25 (3.7)	29 (5.3)	21 (3.1)	Y			
	54 (7.8)	37 (5.3)	52 (7.5)	43 (6.3)	Z			
ultimate strain	4.0	4.3	8.5	8.4	X	%		
	3.3	3.3	7.7	7.8	Y			
	8.7	8.5	12.5	17.6	Z			
Moisture Absorption	0.02		0.02		N/A	%	.062" (1.6mm) D48/50	ASTM D570
Thermal Conductivity	0.22		0.20		Z	W/m/K	80°C	ASTM C518
Coefficient of Thermal Expansion	22 28 173		31 48 237		X Y Z	ppm/°C	0-100°C	IPC-TM-650, 2.4.41
Td	500		500		N/A	°C TGA	N/A	ASTM D3850
Density	2.2		2.2		N/A	gm/cm^3	N/A	ASTM D792
Copper Peel	27.2 (4.8)		31.2 (5.5)		N/A	pli (N/mm)	1 oz (35mm) EDC foil after solder float	IPC-TM-650 2.4.8
Flammability	V-0		V-0		N/A	N/A	N/A	UL94
Lead-Free Process Compatible	Yes		Yes		N/A	N/A	N/A	N/A

[1] Specification values are measured per IPC-TM-650, method 2.5.5.5 @ ~10GHz, 23°C. Testing based on 1 oz. electrodeposited copper foil. e_r values and tolerance reported by IPC-TM-650 method 2.5.5.5 are the basis for quality acceptance, but for some products these values may be incorrect for design purposes, especially microstrip designs. We recommend that prototype boards for new designs be verified for desired electrical performance.
[2] Typical values should not be used for specification limits, except where noted.
[3] SI unit given first with other frequently used units in parentheses.
[4] The design Dk is an average number from several different tested lots of material and on the most common thickness/s. If more detailed information is required, please contact Rogers Corporation. Refer to Rogers' technical paper "Dielectric Properties of High Frequency Materials" available at http://www.rogerscorp.com.

Standard Thickness	Standard Panel Size	Standard Copper Cladding	Non-Standard Copper Cladding
0.005" (0.127mm) 0.031" (0.787mm) 0.010" (0.254mm) 0.062" (1.575mm) 0.015" (0.381mm) 0.125" (3.175mm) 0.020" (0.508mm) Non-standard thicknesses are available	18" X 12" (457 X 305mm) 18" X 24" (457 X 610mm) Non-standard sizes are available up to 18" X 48" (457 X 1219 mm)	½ oz. (18µm) and 1 oz. (35µm) electrodeposited and rolled copper foil	¼ oz. (9 µm) electrodeposited copper foil ½ oz. (18µm), 1 oz. (35µm) and 2 oz. (70µm) reverse treat copper foil 2 oz. (70µm) electrodeposited and rolled copper foil
		Thick metal claddings may be available based on dielectric and plate thickness. Contact customer service for more information on available non-standard and custom thicknesses, claddings and panel sizes	